https://doi.org/10.5194/egusphere-2024-3860
Preprint. Discussion started: 17 December 2024

Evaluating Nitrogen Oxide and α-pinene Oxidation Chemistry: Insights from Oxygen and Nitrogen Stable Isotopes

Wendell W. Walters[1,2], Masayuki Takeuchi[3,a], Danielle E. Blum[4], Gamze Eris[5], David Tanner[6], Weiqi Xu[5,7], Jean Rivera-Rios[5,b], Fobang Liu[5,8], Tianchang Xu[5], Greg Huey[6], Justin B. Min[6], Rodney Weber[6], Nga L. Ng [3,5,6], and Meredith G. Hastings[2,9]

[1]Department of Chemistry and Biochemistry, University of South Carolina, 631 Sumter St, Columbia, SC 29208, USA
[2]Institute at Brown for Environment and Society, Brown University, 85 Waterman St, Providence, RI 02912, USA
[3]School of Civil and Environmental Engineering, Georgia Institute of Technology, 311 Ferst Drive NW, Atlanta, GA 30332, USA
[4]Department of Chemistry, Brown University, 324 Brook Street, Providence, RI 02912, USA
[5]School of Chemical and Biomolecular Engineering, Georgia Institute of Technology, 311 Ferst Drive NW, Atlanta, GA 30332, USA
[6]School of Earth and Atmospheric Sciences, Georgia Institute of Technology, 311 Ferst Drive NW, Atlanta, GA 30332, USA
[7]State Key Laboratory of Atmospheric Boundary Layer Physics and Atmospheric Chemistry, Institute of Atmospheric Physics, Chinese Academy of Sciences, Beijing, 100029, China
[8]Department of Environmental Science and Engineering, Xi'an Jiaotong University, Xi'an, Shaanxi, 710049, China
[9]Department of Earth, Environmental, and Planetary Sciences, Brown University, 324 Brook Street, Box 1846, Providence, RI 02912, USA

Correspondence to: Wendell W. Walters (wendellw@mailbox.sc.edu)

[a]Now at Department of Mechanical Engineering, University of Colorado Boulder, 1111 Engineering Dr, Boulder, CO, 80309, USA
[b]Now at Department of Chemistry and Chemical Biology, Rutgers University, 123 Bevier Rd, Piscataway, NJ, 08854, USA

Abstract. The chemical interaction between nitrogen oxides (NO_x = NO + NO_2) and α-pinene plays a critical role in air quality and climate. However, uncertainties remain regarding their coupling in NO_x loss, renoxification, and oxidation chemistry. To address these gaps, we conducted controlled chamber experiments, analyzing nitric acid (HNO_3), NO_2, and particulate nitrate (pNO_3) for their oxygen and nitrogen stable isotope variations ($\Delta^{17}O$, $\delta^{18}O$, and $\delta^{15}N$). A strong linear relationship between $\delta^{18}O$ and $\Delta^{17}O$ across experiments revealed contributions of oxygen from ozone (O_3) and atmospheric oxygen (O_2) in forming reactive radicals. The $\delta^{15}N$ values followed the order $\delta^{15}N(pNO_3) < NO_2 < HNO_3$, reflecting isotope fractionation during NO_x oxidation. A new chemical mechanism accurately predicted aerosol precursor decay and simulated $\Delta^{17}O$ and $\delta^{15}N$ values. Simulations showed NO_x photochemical cycling and pNO_3 formation, primarily from organic nitrate, with $\Delta^{17}O(NO_2)$ simulations achieving a root mean square error (RMSE) of 1.7‰. Improved $\delta^{15}N(NO_2)$ and pNO_3 simulations used a nitrogen isotope fractionation factor ($^{15}\alpha$) of 0.997 for NO_2 + OH reactions. However, modeling $\Delta^{17}O$ and $\delta^{15}N$ of HNO_3 proved challenging, likely due to sampling artifacts. This study provides insights into $\Delta^{17}O$ transfer dynamics, nitrogen isotope

https://doi.org/10.5194/egusphere-2024-3860
Preprint. Discussion started: 17 December 2024

fractionation, and the role of NO_x-BVOC chemistry in air quality, highlighting the potential of $\Delta^{17}O$ and $\delta^{15}N$ as tools for evaluating complex atmospheric processes.

1 Introduction

The oxidation of biogenic volatile organic compounds (BVOCs) in the presence of nitrogen oxides (NO_x = NO + NO_2) constitutes an important mechanism of coupled biogenic-anthropogenic interactions. This interplay bears significant consequences for air quality, climate, global reactive nitrogen budget, and secondary organic aerosols (SOA) (Hoyle et al., 2011; Ng et al., 2017; Romer et al., 2016; Sato et al., 2022; Takeuchi and Ng, 2019; Xu et al., 2015b, 2020; Zare et al., 2018). Monoterpenes ($C_{10}H_{16}$) are a major class of BVOCs that, upon oxidation, can lead to significant organic nitrate and SOA formation both during daytime and nighttime (Aschmann et al., 2002; Bates et al., 2022; Bell et al., 2022; Fry et al., 2014; Hallquist et al., 1999; Nah et al., 2016; Nozière et al., 1999; Rindelaub et al., 2015). However, significant gaps exist in our comprehension of monoterpene and NO_x coupled chemistry, including the fate of organic nitrogen and its influence on NO_x and oxidant budgets. Once formed, gas-phase organic nitrogen can either photolyze or oxidize, leading to the release of NO_x ("renoxification"), partition into the particle phase, resulting in particulate organic nitrogen production (Beaver et al., 2012; Browne et al., 2014; Browne and Cohen, 2012; Fisher et al., 2016; Wang et al., 2023), and/or undergo dry and wet deposition, leading to the removal of reactive nitrogen from the atmosphere. An important loss process for organic nitrate is hydrolysis in the particle phase, leading to the production of nitric acid (HNO_3) (Day et al., 2010; Rindelaub et al., 2016; Russell et al., 2011; Takeuchi and Ng, 2019; Wang et al., 2021; Zare et al., 2018). Understanding the fates of organic nitrogen and the feedback in oxidation chemistry arising from BVOC/NO_x interactions is critical for accurately assessing their roles in NO_x loss and recycling, O_3 formation, and SOA generation.

To address these fundamental uncertainties and advance our understanding, it is imperative to employ methodologies that can be used to deduce the reaction mechanisms governing the formation and fate of organic nitrogen. The natural variations of stable oxygen and nitrogen isotopes in various reactive nitrogen (NO_y = NO_x + HNO_3 + alkyl nitrate ($RONO_2$) + peroxy nitrate (RO_2NO_2) + etc.) molecules may be a promising analytical tool to enhance our insight into the intricate connections between NO_x and BVOC chemistry and their implications for atmospheric composition (Michalski et al., 2012; Walters et al., 2018). Stable isotope approaches offer novel avenues to probe and refine our understanding of complex atmospheric processes, unravel the dynamics of BVOC/NO_x interactions, and ultimately contribute to formulating informed air quality management strategies.

Variations in oxygen (O) isotope ratios (i.e., $^{18}O/^{16}O$ and $^{17}O/^{16}O$), commonly quantified using isotope delta notation ($\Delta^{17}O$ and $\delta^{18}O$), offer a powerful proxy for assessing oxidation pathways involving NO_x photochemical cycling and nitrate formation

https://doi.org/10.5194/egusphere-2024-3860
Preprint. Discussion started: 17 December 2024

(Albertin et al., 2021; Alexander et al., 2020; Michalski et al., 2003; Morin et al., 2011; Walters et al., 2024b). This is owing to distinct $\Delta^{17}O$ and $\delta^{18}O$ values exhibited by key atmospheric oxidants, which are proportionally transferred to NO_x during oxidation in the atmosphere (Hastings et al., 2003; Michalski et al., 2003). For instance, tropospheric O_3 has an elevated $\Delta^{17}O$ with a mean value near 26‰, and the transferable terminal oxygen atom of O_3 (O_3^{term}) exhibiting a $\Delta^{17}O$ of 39.3 ± 2‰ and elevated $\delta^{18}O$ near 126±12‰ based on recent near-surface observations (Ishino et al., 2017; Vicars and Savarino, 2014). In contrast, other atmospheric oxidants such as RO_2/HO_2 and OH have $\Delta^{17}O$ values at or near 0‰ (Lyons, 2001; Walters et al., 2024a). The $\delta^{18}O$ values of RO_2/HO_2 and OH have not been directly determined but are anticipated to be lower than the $\delta^{18}O(O_3^{term})$ (Michalski et al., 2012). The $\Delta^{17}O$ isotopic differences provide quantitative measures to evaluate NO_x photochemical cycling and nitrate formation processes. Notably, $\Delta^{17}O$ has been frequently utilized to assess atmospheric nitrate formation pathways, as different pathways yield distinct $\Delta^{17}O$ values based on oxygen isotope mass-balance assumptions (Alexander et al., 2020; Michalski et al., 2003; Morin et al., 2011; Walters et al., 2024b). More recent advancements include the first reliable *in situ* measurements of $\delta^{18}O(NO_2)$ and $\Delta^{17}O(NO_2)$, which enable an evaluation of NO_2 formation pathways (i.e., NO + O_3 vs NO + RO_2/HO_2) (Albertin et al., 2021; Walters et al., 2018, 2024b). Further, we have recently developed a chemical mechanism that can explicitly model $\Delta^{17}O$ of numerous NO_y components, termed InCorporating Oxygen Isotopes of Oxidized Reactive Nitrogen (ICOIN) based on the Regional Atmospheric Chemistry Mechanism, Version 2 mechanism (RACM2) (Walters et al., 2024a). These new tools offer exciting opportunities for probing NO oxidation branching ratios, assessing organic nitrogen yields from NO + RO_2 reactions under various NO_x/BVOC conditions, and evaluating nitric acid formation mechanisms including both inorganic and organic reaction pathways.

The stable nitrogen (N) isotope ratio variations ($\delta^{15}N$) of NO_x and atmospheric nitrate have conventionally served as a valuable proxy for evaluating precursor emission sources, because of the preserved N mass between the precursor and oxidized end-products (Elliott et al., 2019; Hastings et al., 2013). However, it is essential to consider that NO_x photochemical cycling and atmospheric nitrate formation processes can also induce significant mass-dependent fractionation effects (Freyer et al., 1993; Li et al., 2020; Walters et al., 2016; Walters and Michalski, 2015, 2016). Field $\delta^{15}N$ observations of NO_2 and nitrate have demonstrated the potential of these fractionation effects to offer additional valuable information concerning NO_x photochemical cycling and atmospheric nitrate formation (Albertin et al., 2021; Bekker et al., 2023; Li et al., 2021; Walters et al., 2018). Recently, a novel chemical mechanism was devised to model the nitrogen isotope fractionation associated with NO_x chemistry, called incorporating ^{15}N into the Regional Atmospheric Chemistry Mechanism (i_NRACM) (Fang et al., 2021). Leveraging these advancements, we may utilize $\delta^{15}N$ to gather supplementary quantitative insights into BVOC/NO_x interactions and their impact on organic nitrogen fates and contributions to HNO_3 formation.

This study presents the first $\Delta^{17}O$, $\delta^{18}O$, and $\delta^{15}N$ values of several simultaneously collected NO_y species, including NO_2, HNO_3, and pNO_3, from controlled laboratory experiments involving α-pinene, the most abundant monoterpene. These experiments were conducted under diverse oxidant conditions to investigate distinct RO_2 fates, enabling a comprehensive

https://doi.org/10.5194/egusphere-2024-3860
Preprint. Discussion started: 17 December 2024

evaluation of the impact of BVOC/NO_x interactions on atmospheric oxidant budgets, organic nitrogen fates, and NO_x loss and/or recycling. The $\Delta^{17}O$ and $\delta^{15}N$ of the various NO_y components were simulated utilizing recently developed isotope mechanism frameworks (Fang et al., 2021; Walters et al., 2024a), yielding invaluable insights into the formation mechanisms and fates of NO_x, HNO_3, and organic nitrogen under varying oxidant conditions. Additionally, this approach tremendously aids in our understanding of $\Delta^{17}O$ transfer dynamics as well as $\delta^{15}N$ fractionation patterns associated with NO_x oxidation chemistry.

2 Methods

2.1 Chamber Experiments

Photochemical and nighttime oxidation chamber experiments were conducted involving α-pinene, NO_x, and oxidant precursors at the Georgia Institute of Technology Environmental Chamber Facility that houses two 12 m^3 Teflon reactors (Boyd et al., 2015). A total of six different initial experimental conditions were targeted, including five photochemical and one nighttime condition as previously reported (Blum et al., 2023) (Table 1). The experiments varied in their precursor concentrations and oxidant types, which were utilized to probe different α-pinene oxidation reactions involving OH, O_3, and nitrate radical (NO_3) and alkylperoxy radical (RO_2) fates. Replicates were conducted in two of the targeted experimental conditions. The conducted chamber experiments follow well-established laboratory protocols and experimental conditions (Boyd et al., 2015; Nah et al., 2016; Takeuchi and Ng, 2019; Tuet et al., 2017). Briefly, photochemical experiments were conducted by injecting dry ammonium sulfate seed aerosol and precursor (i.e., α-pinene (99% Sigma-Aldrich)), NO (Matheson), hydrogen peroxide (H_2O_2), or nitrous acid (HONO)) into the chamber, where either H_2O_2 or HONO was used as an OH precursor to simulate different extents of RO_2+NO pathway. Once the levels of precursors stabilized, the chamber lights were turned on, signifying the start of the photochemical experiments. The procedure used to generate HONO (e.g., the reaction of sodium nitrite with sulfuric acid) also leads to the generation of significant NO and NO_2 as a reaction by-product (Kroll et al., 2005; Tuet et al., 2017). For simulated nighttime conditions, dry ammonium sulfate seed aerosol and α-pinene were injected into the chamber, followed by flowing dinitrogen pentoxide (N_2O_5) for fifteen minutes (Boyd et al., 2015; Takeuchi and Ng, 2019). The N_2O_5 injection corresponded to the start of the nighttime experiments. The N_2O_5 was generated by reacting NO_2 from a gas cylinder (Matheson) with O_3 in a flow tube prior to the introduction to the chamber at a ratio of 2:1 to minimalize O_3 concentrations in the chamber to avoid ozonolysis. All experiments were conducted at a relative humidity (RH) and temperature of 30 % and 22 °C, respectively. Before each experiment, the chamber was flushed with zero air and irradiated for at least 24 hours.

https://doi.org/10.5194/egusphere-2024-3860
Preprint. Discussion started: 17 December 2024

Table 1. Summary of measured NO_y precursor concentrations and targeted H_2O_2 concentrations for the chamber experiments. All experiments were conducted using dry ammonium sulfate seed at a fixed temperature (22°C) and relative humidity (30%). The experiments were conducted using two different chambers designated as A and B.

Experiment	*α*-pinene (ppb)	NO_y (ppb)	Oxidant (ppb)
1	298	NO^a = 55.3 HNO_3^d = 5.1	H_2O_2 = 9,000
1R	297	NO^a = 49.5 HNO_3^d = 3.5	H_2O_2 = 9,000
2	290	NO^a = 112 HNO_3^d = 3.18	H_2O_2 = 6,000
3	286	NO^a = 338 HNO_3^d = 4.77	H_2O_2 = 6,000
4	293	NO^a = 615 HNO_3^d = 5.74	H_2O_2 = 4,500
4R	316	NO^a = 655 HNO_3^d = 5.51	H_2O_2 = 4,500
5	306	$HONO^b$ = 210 NO^b = 320 NO_2^b = 460 HNO_3^d = 9.08	N/A
6	100	NO_2, NO_3, N_2O_5, HNO_3, O_3 = d HNO_3 = 10.0	N/A

[a]The starting NO was assumed to have a $\Delta^{17}O$ = 0‰ and $\delta^{15}N$ = -70.0‰

[b]The starting HONO, NO, and NO_2 were assumed to have $\Delta^{17}O$ = 0‰ and $\delta^{15}N$ = -5.9‰

[c]The chamber HNO_3 "blank" was assumed to have $\Delta^{17}O$ = 26‰ and $\delta^{15}N$ = -35‰.

[d]The emission rate of NO_2, NO_3, N_2O_5, HNO_3, and O_3 into the chamber for a 20 minute injection period were modeled based on a flow tube simulation of the reaction of NO_2 with O_3 with a residence time of 70 s. The initial NO_2 was assumed to have a $\Delta^{17}O$ = 0‰ and $\delta^{15}N$ = -40.5‰

Continuous online measurements of NO, NO_2, and O_3 were conducted using chemiluminescence (Teledyne 200EU), cavity-attenuated phase shift (CAPS), and an O_3 monitor (Teledyne T400). A chemical ionization mass spectrometer (CIMS) was used for various NO_y measurements including HONO and HNO_3 (Huey et al., 1998). The *α*-pinene decay was monitored using gas-chromatography flame ionization detector (GC-FID; Agilent 7890A). Organic nitrate were monitored using a filter inlet for gases and AEROsols (FIGAERO) coupled to a high-resolution time-of-flight iodide chemical ionization mass spectrometer (HR-ToF-I-CIMS) with particles collected on a Teflon filter (Lopez-Hilfiker et al., 2014; Nah et al., 2016; Takeuchi et al., 2022; Takeuchi and Ng, 2019; Wang et al., 2023). Aerosol composition was measured using a high-resolution time-of-flight aerosol mass spectrometer (HR-ToF-AMS) that included measurement of non-refractory organics (Org), sulfate (SO_4), nitrate

https://doi.org/10.5194/egusphere-2024-3860
Preprint. Discussion started: 17 December 2024

(NO_3), and ammonium (NH_4) (DeCarlo et al., 2006; Farmer et al., 2010). Water-soluble aerosol components were also measured using a particle-into-liquid sampler (PILS) coupled to ion chromatography (IC) (Orsini et al., 2003).

Collections of various NO_y gaseous and aerosol components, including HNO_3, NO_2, and pNO_3 were conducted using a modified version of the ChemComb Speciation Cartridge (CCSC) with an extended denuder body for offline concentration and isotope composition analysis (Blum et al., 2020, 2023). Briefly, the CCSC collections began when the aerosol mass spectrometer data indicated the nitrate and secondary organic aerosol mass concentrations had peaked. The CCSC samples were collected at 8 L min^{-1} for up to 4 h. To maintain the chamber integrity, zero-air was used to dilute at 25 L min^{-1} once aerosol peak was reached and CCSC sample collection initiated. The CCSC denuder bodies were replaced one to four times depending on the concentration of NO_x in the chamber. For each experiment, a single filter was used in the CCSC. In addition to the chamber experiments, samples were collected directly from the NO_2 tank (Matheson), which was used in the generation of N_2O_5 for the nighttime oxidation experiments.

Honeycomb denuders were coated for the selective collection of HNO_3 (captured as nitrate (NO_3^-)) and NO_2 (captured as nitrite (NO_2^-)). A detailed description of the coating solutions, denuder preparation, and denuder extraction was previously described, and the pooled isotope reproducibility for both HNO_3 and NO_2 was ±1.7‰, ±1.8‰, and ±0.7‰, for $\delta^{15}N$, $\delta^{18}O$, and $\Delta^{17}O$ (Blum et al., 2023) for these chamber experiments. The collection of $PM_{2.5}$ was conducted using a quartz filter (Cytiva Whatman, Grade QM-A; 47 mm diameter) that was housed in the ChemComb filter cartridge positioned downstream of the denuders. Before use, the quartz fiber filters were placed in a furnace at 550 °C overnight and stored in an airtight container. The filter samples were extracted in 20 mL of Milli-Q water (>18.2 MΩ) and allowed to leach for at least one week at room temperature. This method was conducted to enable hydrolysis of collected organic nitrate particles as previous studies have shown organic nitrate derived from α-pinene oxidation to hydrolyze to NO_3^- in water with a lifetime of 8.8 h at pH = 6.9 (Rindelaub et al., 2016) and 2.5 h at pH = 7.44 (Wang et al., 2021). Other types of organic nitrate, such as secondary nitrates, have been reported to be stable in water, especially at a neutral pH (Wang et al., 2021). The efficiency of our filter extraction technique for organic nitrate hydrolysis was evaluated using the online AMS and PILS data. After the filters were leached, the filters were removed, and the samples were shipped to Brown University where they were placed in a freezer until subsequent concentration and isotope analysis. For all sample media types, including denuders and filters, lab blanks were frequently taken. These blanks were prepared, handled, and analyzed the same way as all samples.

2.2 Concentration and Isotope Analysis

The denuder and filter extracts were analyzed for their NO_2^- and NO_3^- content using a standardized colorimetric technique (e.g., EPA Methods 353.2) or ion chromatography, as previously described (Blum et al., 2020, 2023). The limits of detection (LOD) were approximately 0.1 μmol L^{-1} and 0.3 μmol L^{-1} for NO_2^- and NO_3^- via colorimetric analysis and 3.0 μmol L^{-1} for

https://doi.org/10.5194/egusphere-2024-3860
Preprint. Discussion started: 17 December 2024

NO_2^- via ion chromatography. For all analyses, the average percent relative standard deviation was below 5%. The NO_2^- and NO_3^- concentrations from denuder blank extractions used for NO_2 (n = 5) and HNO_3 (n = 5) collection were below detection limits. Significant blanks were observed in the quartz filter extracts (1.5±0.2 μmol L^{-1}; n = 5).

The $\delta^{15}N$, $\delta^{18}O$, and $\Delta^{17}O$ isotope compositions were analyzed using the denitrifier method for NO_3^- samples and the sodium azide in an acetic acid buffer method for NO_2^- samples (Casciotti et al., 2002; McIlvin and Altabet, 2005; Sigman et al., 2001; Walters and Hastings, 2023). Briefly, these methods produce N_2O from NO_3^- and/or NO_2^-, which is extracted, purified, concentrated, and injected into a continuous flow isotope ratio mass spectrometer for $\delta^{15}N$ and $\delta^{18}O$ determination from *m/z* measurement at 44, 45, and 46. In a separate batch analysis, the generated N_2O is decomposed to O_2 and analyzed for $\Delta^{17}O$ determination from *m/z* measurement at 32, 33, and 34. The samples were calibrated with respect to internationally recognized NO_3^- standards (IAEA-NO-3, USGS35, USGS34) or NO_2^- reference materials (RSIL-N7373 and RSIL-10219) (Böhlke et al., 2003, 2007). The pooled standard deviations of the standards were ±0.1‰ and ±0.6‰ for $\delta^{15}N$ and $\delta^{18}O$ of the NO_3^- standards (n = 78) and ±0.3‰ and ±0.3‰ for $\delta^{15}N$ and $\delta^{18}O$ of the NO_2^- reference materials (n = 15), respectively. The $\Delta^{17}O$ had a pooled standard deviation of ±0.6 ‰ (n = 53) .

All isotope measurements were reported relative to reference standards using delta (δ) notation (Eq. 1):

$$\delta = \left(\frac{{}^{x}R_{sample}}{{}^{x}R_{reference}} - 1\right) \quad \text{(Eq. 1)}$$

where x refers to the heavy isotope (i.e., ^{15}N, ^{18}O, or ^{17}O) and R refers to the ratio of the heavy to the light isotope (i.e., $^{15}N/^{14}N$, $^{18}O/^{16}O$, or $^{17}O/^{16}O$), for the sample or the reference material. The nitrogen and oxygen reference material includes atmospheric air and Vienna Standard Mean Ocean Water (VSMOW), respectively. Oxygen isotope mass-independence ($\Delta^{17}O$) was quantified using the linear definition with a mass-dependent coefficient of 0.52, which is approximately representative of oxygen mass-dependent coefficients expected and observed in nature (Young et al., 2002) (Eq. 2):

$$\Delta^{17}O = \delta^{17}O - 0.52 \times \delta^{18}O \quad \text{(Eq. 2)}$$

The linear $\Delta^{17}O$ approximation is commonly used to describe large mass-independent effects such as those related to O_3 reactions, and this definition is commonly used in the atmospheric chemistry community to track the influence of O_3 oxidation and $\Delta^{17}O$ propagation into reactive components (Alexander et al., 2020; Kim et al., 2022; Michalski et al., 2003; Savarino et al., 2013).

2.3 Data Reduction and Corrections

Due to significant NO_3^- blanks found in the pNO_3 filter extracts, the measured $\delta^{15}N$, $\delta^{18}O$, and $\Delta^{17}O$ were corrected based on mass-balance (Eq. 3-4):

$$\delta(\text{corrected}, pNO_3) = \frac{\delta(\text{measure}) - (f(\text{blank}) \times \delta(\text{blank}))}{1 - f(\text{blank})} \quad \text{(Eq. 3)}$$

https://doi.org/10.5194/egusphere-2024-3860
Preprint. Discussion started: 17 December 2024

$$f(\text{blank}, \text{pNO}_3) = \frac{[\text{NO}_3^-(\text{blank})]}{([\text{NO}_3^-(\text{blank})]+[\text{NO}_3^-(\text{sample})])} \quad \text{(Eq. 4)}$$

where [NO_3^-], corresponds to the concentration of NO_3^- in either the blank or sample, and *f*(blank) corresponds to the fraction of NO_3^- that corresponds to the blank. The quartz filter extracts had $\delta^{15}N$, $\delta^{18}O$, and $\Delta^{17}O$ values of 1.6±1.1‰, 16.6±1.4‰, and 3.4±0.5‰, respectively (n = 3). Blank corrections were made for all samples when *f*(blank) was less than 30%. Samples with an *f*(blank) that exceeded 30% were not reported for their isotope compositions, which included 1 out of 8 quartz filter extracts. The uncertainty in the blank corrected isotope deltas was calculated using a Monte-Carlo simulation for 10,000 iterations and assuming a normal distribution using Matlab. For the quality assurance criterion of an *f*(blank) < 30%, the uncertainties were calculated to be less than 4.1‰, 1.4‰, and 0.9‰ for $\delta^{15}N$, $\delta^{18}O$, and $\Delta^{17}O$, respectively.

2.4 Aerosol Nitrate Composition

The relative contribution of organic aerosol nitrate (pNO_3(Org)) to the total pNO_3 was determined from two approaches. First, the relative proportion of pNO_3(Org), was calculated based on NO^+ and NO_2^+ HR-ToF-AMS fragmentation as previously described (Farmer et al., 2010; Fry et al., 2009; Kiendler-Scharr et al., 2016; Xu et al., 2015a) (Eq. 5):

$$f(\text{pNO}_3, \text{Org}) = \frac{(R_{\text{obs}}-R_{\text{AN}})(1+R_{\text{ON}})}{(R_{\text{ON}}-R_{\text{AN}})(1+R_{\text{obs}})} \quad \text{(Eq. 5)}$$

where *f*(pNO_3, Org) refers to the fraction of pNO_3(Org) to the total pNO_3, R refers to NO^+/NO_2^+ fragments, and obs, AN, and ON refers to the observed, ammonium nitrate, and organic nitrate, respectively. The R_{AN} was obtained from routine ionization efficiency calibration of the HR-ToF-AMS using 300 nm ammonium nitrate aerosols and was 1.37. The R_{ON} was calculated based on the measured R_{AN} and the ratio of R_{ON}/R_{AN} previously reported for similar conducted experiments (Takeuchi and Ng, 2019), resulting in an R_{ON} of 2.70±0.29 and 3.86±0.34 for photochemical and nighttime oxidation experiments, respectively. The second method for qualitatively determining *f*(pNO_3, Org) involved evaluating the relative change in the molar ratio of NH_4/SO_4, as an increase in NH_4/SO_4 has been observed to be associated with inorganic pNO_3 formation (Takeuchi and Ng, 2019).

2.5 Box Model Simulations

The chamber experiments were simulated using the Framework for 0-D Atmospheric Modeling (F0AM) box model (Wolfe et al., 2016). The model was initiated for each experiment using the measured precursor concentrations for NO, NO_2, HONO, and α-pinene before chamber lights were turned on or N_2O_5 was injected and using the targeted H_2O_2 concentrations. Additionally, a "chamber blank" of HNO_3, based on the CIMS measurements, was present before the start of the experiment (Fig. S1). To accurately reflect this condition in the model, an initial concentration of HNO_3 was included in the experimental simulations based on the observed CIMS measurements (Table 1). The pressure, temperature, and relative humidity were fixed at 1013 mbar, 295 K, and 30%, respectively. The measured chamber light flux data was used. The model was run in two parts for the photochemical reactions, including from lights on to peak SOA mass concentration (part 1) and from aerosol decay and chamber dilution to the end of NO_y collections (part 2). For the nighttime experiments, the model simulations were conducted

https://doi.org/10.5194/egusphere-2024-3860
Preprint. Discussion started: 17 December 2024

in three parts, including from the start of N_2O_5 injection to the end of N_2O_5 injection (part 1), from the end of N_2O_5 injection to peak SOA mass concentrations (part 2) and from the decay of organic aerosol and chamber dilution to the end of NO_y collection (part 3). The N_2O_5 injection was simulated by first modeling the NO_2 reaction with O_3 in the flow tube, considering a flow tube residence time of 70 s. The nighttime experiment was then simulated by allowing the flow tube products (i.e., NO_2, O_3, NO_3, HNO_3, and N_2O_5) to emit into the chamber for 20 minutes (part 1). Next, the experiment was modeled without the flow tube emission to the start of aerosol decay and chamber dilution (part 2) and from aerosol decay and chamber dilution to the end of NO_y collections (part 3). For both photochemical and nighttime experiments, the model simulations from the decay of organic aerosol to the end of NO_y collection included a chamber dilution rate of $k_{dil} = 8.00 \times 10^{-5}$ s^{-1}, which was determined based on accurately matching the decay of NO for the photochemical experiments with the highest levels of initial starting NO_y (i.e., Exp. 4, and 5).

A new chemical mechanism was developed, termed University of South Carolina α-pinene (USC-API), to accurately model the oxidation of NO_x and α-pinene (Table S1-S2). This mechanism was developed due to difficulties in simulating the initial decay of the aerosol precursors including α-pinene, NO, NO_2, and HONO for the various experiment conditions using either the Regional Atmospheric Chemical Mechanism, v2 (RACM2; (Goliff et al., 2013) or the Master Chemical Mechanism v3.3.1 (Jenkin et al., 1997; Saunders et al., 2003). The USC-API mechanism focuses on simulating α-pinene and NO decay along with NO_x oxidation but does not intend to accurately simulate SOA production and later-generation chemistry. The mechanism includes the inorganic reactions included in RACM2, including 16 species and 45 reactions. It also incorporates 29 organic species and 61 reactions to detail organic chemistry up to one generation past pinonaldehyde formation as well as the formation of pinonaldehyde derived peroxyacetyl nitrate formation, with subsequent chemistry represented by a lumped approach. The α-pinene oxidation pathways involving OH, O_3, and NO_3, along with specific reactions of the resulting RO_2 with HO_2, NO, NO_3, and other RO_2 radicals, are included. The photochemical oxidation of α-pinene largely follows the MCMv3.3.1 (Saunders et al., 2003), incorporating two hydroxyl-nitrate isomers from $OH/O_2/NO$, including one teritary (ONITa) and one secondary (ONITb) and the formation of a tertiary pinene carbonyl nitrate (ONITc). Nighttime oxidation chemistry integrates a recent mechanism for organic nitrate formation, producing pinene nitrate hydroperoxide, including one tertiary (ONITOOHa) and one secondary (ONITOOHb) via HO_2 reactions and dimer/pinene dinitrate (PDN) through RO_2 interactions (Bates et al., 2022). Product yields for organic nitrate were adjusted based on experimental isotope data, accounting for $OH/O_2/NO$ and NO_3 pathways, which can be elucidated based on a comparison to $\Delta^{17}O$ (Walters et al., 2024b).

The $\Delta^{17}O$ of NO_y compounds were simulated using the newly developed USC-API mechanism modified using the InCorporating Oxygen Isotopes of oxidized reactive Nitrogen in the Regional Atmospheric Chemistry Mechanism, Version 2 (ICOIN-RACM2) model framework (Walters et al., 2024a). Briefly, the model framework tracks the transfer and propagation of $\Delta^{17}O$ from O_3 into NO_y and O_x species. This mechanism tags the oxygen atoms transferred from O_3 into NO_y and O_x

https://doi.org/10.5194/egusphere-2024-3860
Preprint. Discussion started: 17 December 2024

considering mass-balance and reaction stoichiometry and enables the offline calculation of $\Delta^{17}O$ based on the output of concentrations of various NO_y and HO_x isotopologues (Eq. 6):

$$\Delta^{17}O(X) = f(Q) \times \Delta^{17}O(O_3^{term}) \quad \text{(Eq. 6)}$$

where X refers to the various NO_y and O_x molecules and f(Q) is the fractional number of oxygen-atoms deriving from O_3 for a particular molecule. The $\Delta^{17}O(O_3^{term})$ represents the $\Delta^{17}O$ value of the terminal and transferrable O atom of O_3, which was assumed to be 39±2‰ based on recent near-surface collections of O_3 (Ishino et al., 2017; Vicars and Savarino, 2014) and O_3 generated from O_2/NO_x photochemical experiments conducted under normal temperature and pressure conditions (Michalski et al., 2014). The initial $\Delta^{17}O(NO)$ and $\Delta^{17}O(NO_2)$ was set to 0‰, while the initial $\Delta^{17}O(HNO_3)$ from the "chamber blank" was set to 26‰, representing 2/3 O-atoms derived from O_3. This value was not measured but assumed based on the measured $\Delta^{17}O(HNO_3)$ for Exp. 1 and 2, in which the HNO_3 "chamber blank" significantly contributed to the total produced experimental HNO_3, up to approximately 20% (Fig. S1).

Additionally, $\delta^{15}N$ of NO_y molecules were also simulated by adapting the framework from the recently developed isotope variant of the RACM2 mechanism, termed i_NRACM: incorporating ^{15}N into the Regional Atmospheric Chemistry Mechanism (Fang et al., 2021). The model framework explicitly tracks the ^{15}N and ^{14}N abundance of various NO_y molecules and includes nitrogen isotope fractionation associated with NO_x oxidation. The $\delta^{15}N$ of various NO_y components is then calculated using a $^{15}N/^{14}N$ ratio of 0.003677 for air. The $\delta^{15}N$ chamber simulations were initiated with starting concentrations for the nitrogen isotopologues depending on the initial NO_y source. For the nighttime oxidation experiments that used NO_2 as the initial NO_y source (Exp. 6), the starting $\delta^{15}N(NO_2)$ was set to -40.5‰, which was the measured value from the NO_2 source (Matheson NO_2 tank) (-40.5±0.5‰; n = 3). For the experiments that initialize experiments using NO (Exp. 1-4), a $\delta^{15}N(NO)$ value of -70.0±1.4‰ was assumed based on previous measurements from a commercially available tank of NO (Fibiger et al., 2014). Finally, for the HONO experiments (Exp. 5), a $\delta^{15}N(HONO)$ value of -5.9±0.5‰ was assumed based on the lab generation of HONO in a previous study, following a similar methodology as utilized in this study (Chai and Hastings, 2018). Additionally, the "chamber blank" $\delta^{15}N(HNO_3)$ was set to -35‰, which was the average of the photochemical experiments using H_2O_2 and a high initial NO concentration (Exp. 4).

The base chemistry in all of the model simulations is identical and the tagging of the isotope tracers does not impact the model chemistry (Fang et al., 2021; Walters et al., 2024a). All model simulations were conducted without considering chamber wall-loss. Additionally, these are gas-phase mechanisms and do not explicitly model heterogeneous reactions or aerosol chemistry. Further, given the low relative humidity conditions and dry aerosol seed conditions, organic nitrate hydrolysis was not included in the initial model. The chemical mechanism performance in simulating $\Delta^{17}O$ and $\delta^{15}N$ values and thus oxidation chemistry was evaluated using the RMSE metric (Eq. 7):

$$RMSE = \sqrt{\frac{1}{n}\sum_{i=1}^{n}(\delta_o - \delta_m)^2} \quad \text{(Eq. 7)}$$

https://doi.org/10.5194/egusphere-2024-3860
Preprint. Discussion started: 17 December 2024

where δ_o are the isotope observations, δ_m are the model simulated values, and n is the number of observations. Adjustments to the model chemistry were conducted to reduce the RMSE values.

3. Results and Discussion

3.1 Isotope Observations

3.1.1 $\Delta^{17}O$ and $\delta^{18}O$ of NO_y

There was a significant relationship between $\delta^{18}O$ and $\Delta^{17}O$ across NO_y species ($\delta^{18}O = (11.1\pm1.0) + (2.42\pm 0.04)\times\Delta^{17}O$; r = 0.992 ; $p < 0.01$) (Fig. 1). The strong linear relationship between $\delta^{18}O$ and $\Delta^{17}O$ indicates that the oxygen isotopes of the various collected NO_y compounds derived between two dominant pools of O-sources, with high and low $\delta^{18}O$ and $\Delta^{17}O$ values that were consistent across all experimental conditions. The high-end member $\delta^{18}O$ and $\Delta^{17}O$ source can reasonably be assumed to derive from O_3^{term}. Assuming a $\Delta^{17}O(O_3^{term})$ value of 39.3±2.0 ‰ (Ishino et al., 2017; Michalski et al., 2014; Vicars and Savarino, 2014), would indicate a $\delta^{18}O$ transferred from O_3^{term} to the NO_y products of 106±5.0‰. Assuming the low-end member O-source to have a $\Delta^{17}O$ of 0‰, indicates a $\delta^{18}O$ value of 11.1±1.0‰ transferred into the NO_y products that could be reasonably be expected to derive from RO_2, HO_2, and OH radicals. The $\delta^{18}O$ of RO_2/HO_2 radicals has previously been suggested to be near $\delta^{18}O(O_2)$ (Michalski et al., 2012). Indeed, the derived $\delta^{18}O$ value of 11.8±1.0‰ is near the atmospheric $\delta^{18}O(O_2)$ value of 23.2 ‰ (Craig, 1957), which should be near the O_2 in the chamber that was from a zero-air generator. Slight differences between these values could be due to kinetic isotope effects associated RO_2/HO_2 reactions. In addition to RO_2/HO_2 radicals, the OH radical plays an important role in the photochemical formation of HNO_3 and would be expected to proportionally transfer its O atom to the HNO_3 product.

The $\Delta^{17}O$ and $\delta^{18}O$ values increased in the order $pNO_3 < HNO_3 < NO_2$. The $\Delta^{17}O$ and $\delta^{18}O$ of NO_2, HNO_3, and pNO_3 were sensitive to the types of experiments and their oxidant conditions. For example, NO_2 samples collected during the photochemical experiments (i.e., Exp. 1-5) indicated that $\delta^{18}O(NO_2)$ and $\Delta^{17}O(NO_2)$ increased with the initial [NO_y], the ratio of initial [NO_y]:[BVOC], and with decreasing initial [H_2O_2]. These sensitivities to $\delta^{18}O(NO_2)$ and $\Delta^{17}O(NO_2)$ reflect the balance between NO branching ratios involving O_3 vs RO_2/HO_2 (Albertin et al., 2021; Walters et al., 2018). Thus, the relative branching ratios of $NO+O_3$ and $NO+RO_2/HO_2$ changed with experimental photochemical conditions, favoring a greater proportion of $NO+O_3$ reactions for higher initial NO_y and lower [H_2O_2] conditions. For the nighttime oxidation experiment (Exp. 6), the $\Delta^{17}O$ and $\delta^{18}O$ reflected the initial production of N_2O_5 from the oxidation of NO_2 (from a gas cylinder) with O_3. The expected $\Delta^{17}O$ and $\delta^{18}O$ values can be calculated assuming N_2O_5 equilibrium between NO_3 and NO_2 (i.e., $N_2O_5 \rightleftharpoons NO_2 + NO_3$) and using O isotope mass balance (Eq. 8):

$$\delta(NO_2) = \frac{1}{5}\left(\delta(O_3^{term})\right) + \frac{4}{5}\left(\delta(NO_2^{tank})\right) \quad \text{(Eq. 8)}$$

https://doi.org/10.5194/egusphere-2024-3860
Preprint. Discussion started: 17 December 2024

where δ refers to either $\Delta^{17}O$ or $\delta^{18}O$, O_3^{term} refers to the O-atom at the terminal end of O_3 and NO_2^{tank} refers to the NO_2 from the tank source with measured $\Delta^{17}O$ and $\delta^{18}O$ values of -0.1±0.1 ‰ (n=3) and 13.1±0.2‰ (n=3), respectively. Using the assumed $\Delta^{17}O(O_3^{term})$ of 39.3 ± 2.0‰, and the calculated $\delta^{18}O(O_3^{term})$ incorporated into NO_y (106±5.0‰) we would estimate the $\Delta^{17}O$ and $\delta^{18}O$ of NO_2 for the nighttime oxidation experiment to be 7.7 ±0.4‰ and 31.7±1.0‰, respectively, which was near their measured values from the nighttime chamber experiments of (7.2±0.2‰) and (31.9±0.7‰) (n = 3), respectively.

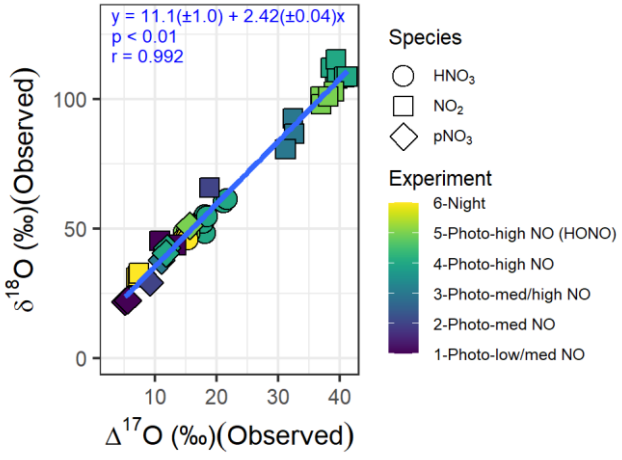

Fig. 1. The observed oxygen isotope delta values of various NO_y species (i.e., HNO_3, NO_2, and pNO_3) from the α-pinene/NO_y oxidation experiments. A strong linear correlation (blue line) was observed between $\delta^{18}O$ and $\Delta^{17}O$.

3.1.2 $\delta^{15}N$ of NO_y

The $\delta^{15}N$ of all NO_y species exhibited a large range from -90.3 to -4.0‰ (n = 47) (Fig. 2). This large range of $\delta^{15}N$ values were significantly influenced by the $\delta^{15}N$ values of the various initial NO_y sources that included tank NO (Exp. 1-4), HONO (Exp. 5), and tank NO_2 (Exp. 6) (p < 0.01). The experiments using tank-NO had the lowest $\delta^{15}N$ ($\bar{x}$±s) of (-56.1±21.3‰; n = 32), followed by tank-NO_2 of (-34.7±12.2‰; n = 6), and the highest average was for the HONO experiments of (-7.8±5.7 ‰; n = 9). This trend of $\delta^{15}N$ values tracks with the initial measured or assumed $\delta^{15}N$ source value, in which $\delta^{15}N$ of the generated HONO (assumed to be -5.9±0.5‰) (Chai and Hastings, 2018) was higher than the measured NO_2 tank (-40.9±0.2‰; n = 3), and the NO tank (assumed to be -70.0 ±1.4‰) (Fibiger et al., 2014). This finding provides evidence that $\delta^{15}N$ can be used as a qualitative tracer to track NO_x emissions for sources with large differences in their emission $\delta^{15}N$ signatures. However, the experiments also demonstrate large $\delta^{15}N$ fractionation between the various NO_y species for each experiment and initial NO_y source.

https://doi.org/10.5194/egusphere-2024-3860
Preprint. Discussion started: 17 December 2024

Overall, there were significant differences in the $\delta^{15}N$ of the various NO_y species ($p < 0.01$). Overall, $\delta^{15}N(HNO_3)$ that averaged -25.9±13.0‰ (n = 20) were higher than $\delta^{15}N(NO_2)$ that averaged -52.5 ±25.2‰ (n = 20), which were higher than $\delta^{15}N(pNO_3)$ that averaged -72.6±22.9‰ (n = 7). This trend suggests that the produced HNO_3 was associated with a positive isotope fractionation (ε) that favored the preferential formation of ^{15}N into HNO_3 relative to NO_2. The isotope fractionation ($^{15}\alpha$) associated with NO_2 + OH has yet to be directly measured but has been precited in the literature with large differences in the suggested value. For example, $^{15}\alpha(NO_2+OH)$ has been suggested to be 0.997 based on the reduced masse of the transition complex (Freyer, 1991), while it has been predicted to be 1.040 in the i_NRACM mechanism (Fang et al., 2021). The higher precited $^{15}\alpha(NO_2+OH)$ value of 1.040 would be consistent with the trend of elevated ^{15}N in HNO_3 relative to NO_2. The $\delta^{15}N(pNO_3)$ values were lower than $\delta^{15}N(NO_2)$. This difference compared to HNO_3 provides support that the generated pNO_3 did not derive from HNO_3 and instead derived from another source such as organic nitrate. Conversely, the hydrolysis of pNO_3 is likely not a main contributor to HNO_3 due to their large $\delta^{15}N$ differences. The low $\delta^{15}N(pNO_3)$ values would reflect the influence of NO_x isotope exchange, which depletes NO in ^{15}N relative to NO_2 (Freyer et al., 1993; Li et al., 2020; Walters et al., 2016). The ^{15}N depleted NO can then react with α-pinene derived peroxy radicals leading to organic nitrate production with a low $\delta^{15}N$ value relative to $\delta^{15}N(NO_2)$. This trend in $\delta^{15}N(NO_y)$ followed all experiments except for the HONO experiments (Exp. 5), in which $\delta^{15}N(NO_2)$ (-5.8±1.8 ‰; n = 4) were insignificantly different from the $\delta^{15}N(HNO_3)$ (-6.2±0.7‰; n = 4) (p>0.05).

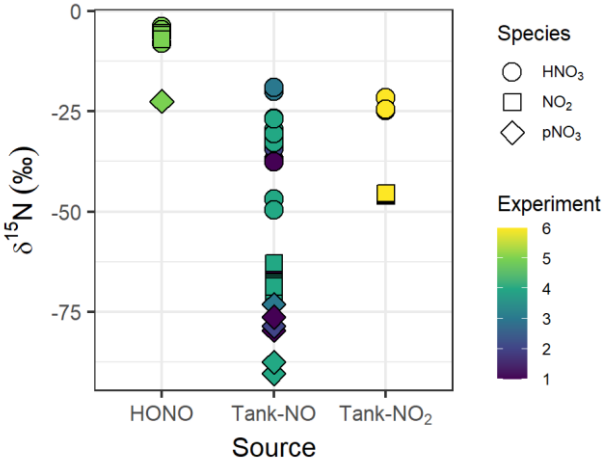

Fig. 2. The observed $\delta^{15}N$ of various NO_y species (i.e., HNO_3, NO_2, and pNO_3) collected during the various conducted α-pinene/NO_y oxidation experiments. The measured $\delta^{15}N$ were sorted by the various starting NO_y sources, including HONO ($\delta^{15}N$ = -5.9±0.5‰), tank-NO ($\delta^{15}N$ = -70.0±1.4‰), and tank-NO_2 ($\delta^{15}N$ = -40.9±0.2‰).

https://doi.org/10.5194/egusphere-2024-3860
Preprint. Discussion started: 17 December 2024

3.2 Particle Nitrate Composition

The generated pNO_3 could have both inorganic (i.e., HNO_3 condensation) and organic (i.e., organic nitrate condensation) contributions. The $\delta^{15}N$ data would indicate that the pNO_3 appeared to derive from a separate source than HNO_3 due to their large $\delta^{15}N$ differences, suggesting that pNO_3 was derived primarily from organic nitrate. We also utilized the HR-ToF-AMS NO^+ and NO_2^+ data to evaluate the contributions of pNO_3 for the experiments. The $f(pNO_3, Org)$ was calculated according to Eq. 5 for each of the conducted experiments (Table 2). Overall, $f(pNO_3, Org)$ was calculated to have a mean of (1.25 ± 0.04; n=8), indicating that the generated pNO_3 derived from organic nitrate. The calculated $f(pNO_3, Org)$ was higher than 1 even when considering uncertainty estimates. This could be due to deriving R_{ON} values from previously reported R_{ON}/R_{AN} ratios from previously conducted α-pinene oxidation experimental conditions conducted utilizing substantially lower initial precursor concentrations by approximately a factor of 10 (Takeuchi and Ng, 2019). Thus, due to the potential uncertainty in our approach in estimating $f(pNO_3, Org)$, the composition of the generated pNO_3 was also investigated using a qualitative approach involving evaluating the relative change in the molar ratio of NH_4/SO_4 from the HR-ToF-AMS (Fig. S2). For each type of experiment, we found the NH_4/SO_4 molar ratio to be consistently near 1.5. This type of NH_4/SO_4 profile is consistent with the generated pNO_3 deriving from organic nitrate, as the dissolution of HNO_3 into aqueous aerosol followed by neutralization with available NH_3 would be expected to lead to an abrupt increase in the molar ratio of NH_4/SO_4 (Takeuchi and Ng, 2019). Overall, both the quantitative and qualitative analysis of pNO_3 composition utilizing the AMS data as well as our $\delta^{15}N$ data indicates that pNO_3 was mainly derived from organic nitrate. Hereinafter, we will assume that the NO_3^- extracted from the filter collections derived from organic nitrate.

Table 2. Summary of the HR-ToF-AMS data including NO^+/NO_2^+ fragmentation data (R_{obs}), calculated $f(pNO_3, Org)$, maximum pNO_3 (Max(pNO_3)). Additionally, we quantified the amount of pNO_3 from the PILS (PILS/AMS) and the filter collection relative to the HR-ToF-AMS (Filter/AMS).

Exp.	R_{obs} ($\bar{x}$±σ)	$f(pNO_3, Org)$ ($\bar{x}$±σ)	Max(pNO_3) ($\mu g\ m^{-3}$)	PILS/AMS (%)	Filter/AMS (%)
1	3.36±0.30	1.26±0.10	13.8	41.8	97.8
1R	3.16±0.21	1.19±0.08	13.3	37.8	83.5
2	3.36±0.13	1.27±0.05	25.9	33.2	105.3
3	3.32±0.21	1.25±0.09	27.4	NA	80.5
4	3.18±0.32	1.20±0.13	25.5	42.1	75.8
4R	3.40±0.33	1.27±0.14	15.0	NA	76.1
5	3.49±0.25	1.31±0.11	24.7	NA	59.5
6	5.63±0.49	1.25±0.11	38.6	NA	7.6

https://doi.org/10.5194/egusphere-2024-3860
Preprint. Discussion started: 17 December 2024

The pNO_3 measured by the HR-ToF-AMS indicated similar profiles for the various types of conducted experiments, in which pNO_3 concentrations peaked and subsequently decayed due to wall loss and chamber dilution (Fig. 3). Overall, the maximum pNO_3 concentrations ranged from 13.3 to 38.6 $\mu g\ m^{-3}$ across the various experiments (Table 2). The lowest maximum pNO_3 corresponded to the experimental conditions with low initial NO_x relative to H_2O_2 and BVOC conditions (i.e., Exp 1). In contrast, the highest maximum pNO_3 occurred during the nighttime oxidation experiments (i.e., Exp 6). The pNO_3 concentrations determined from the HR-ToF-AMS were compared with additional measurement techniques, including the PILS and the filter collections for offline analysis (Fig. 3; Table 2). The PILS pNO_3 measurements were available for 4 out of the 8 conducted experiments and indicated a similar time profile as the HR-ToF-AMS; however, the PILS pNO_3 observations were always lower than the HR-TOF-AMS with the amount of pNO_3 determined from PILS relative to the HR-ToF-AMS (PILS/AMS) ranging between 33.2% to 53.8%. The pNO_3 quantified using filter collection and extraction technique was higher than the PILS and in closer agreement with the HR-ToF-AMS for most of the photochemical experiments. For the photochemical experiments (Exp. 1-5), the pNO_3 determined using the filter collection relative to the HR-ToF-AMS (Filter/AMS) for the photochemical experiments ranged between 59.5 to 105.3% and averaged 86.5±12.35 (n=7). However, the filter collection resulted in nearly negligible pNO_3 for the nighttime oxidation experiments (i.e., Exp. 6).

The pNO_3 concentrations determined using the PILS were always lower than that determined by the HR-ToF-AMS and the offline filter collection technique, which would indicate that that not all the collected pNO_3, which were shown to mainly derive from organic nitrate, were hydrolyzed to $NO_3^-{}_{(aq)}$ within the PILS chamber before quantification via Ion Chromatography. The filter collection and extraction method (i.e., leach in MQ water for 1 week), enabled the successful hydrolysis of the collected pNO_3 to $NO_3^-{}_{(aq)}$ from the photochemical experiments, an important pre-requisite for subsequent isotope analysis. The filter collection technique, however, resulted in near negligible pNO_3 for the nighttime oxidation experiments, limiting our ability to measure the isotope composition of pNO_3 from this experiment. This difference in the efficacy of the offline filter collection technique for pNO_3 characterization between the photochemical and nighttime oxidation experiments could be related to the type of organic nitrate formed during the conducted experiments. The photochemical α-pinene oxidation experiments have been suggested to result in higher relative production of tertiary organic nitrate, while nighttime oxidation leads to a relatively lower fraction of tertiary organic nitrate with estimated values of 62% and 15%, respectively (Zare et al., 2018). Recent work has suggested a hydrolysis lifetime of no more than 30 minutes and a hydrolyzable portion of particulate organic nitrate from α-pinene oxidation experiments between 23-32% and 9-17% for α-pinene + OH and α-pinene + NO_3 reactions, respectively (Takeuchi and Ng, 2019). The offline filter collection and extraction technique matches the trend in which more pNO_3 hydrolyzed for the photochemical experiments compared to the nighttime; however, the filter technique would indicate a higher proportion of potential hydrolysable pNO_3 from photochemical experiment than these previous estimates, though with a different timescale. From these results and comparisons, we speculate that the pNO_3 offline filter measurements to encompass the hydrolysable portion of pNO_3 within a week (as the filter samples were extracted and leached in MQ for at least one week), while the HR-ToF-AMS measurements represent the total pNO_3, and the PILS

https://doi.org/10.5194/egusphere-2024-3860
Preprint. Discussion started: 17 December 2024

measurements correspond to the readily hydrolysable portion of pNO_3. Further, the box model simulations of organic nitrate speciation indicate that the nighttime organic nitrate was dominated by the formation of dimer, pinene dinitrate, as well as secondary hydroxyl-nitrate (Fig. S3). If this speciation is correct, the results would suggest that these types of organic nitrate were not readily hydrolysable.

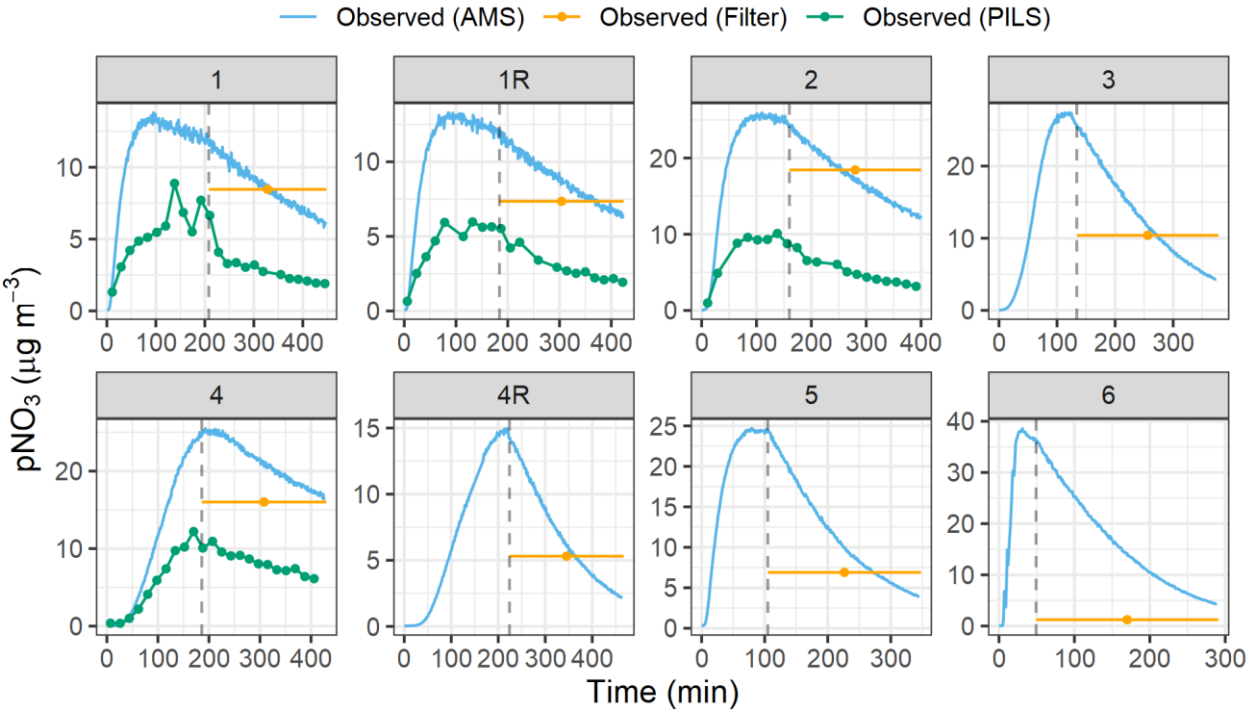

Fig. 3. The observed pNO_3 concentrations are faceted by the various experiments conducted. The concentrations were determined using the High-Resolution Time-of-Flight Aerosol Mass Spectrometer (HR-ToF-AMS), particle-into-liquid sampler (PILS), and filter collection (Filter). The start of the chamber dilution is indicated by the dashed vertical lines, corresponding to the abrupt decrease in pNO_3.

3.3 Model Simulations

3.3.1 Precursor Decay

Box model simulations were conducted to evaluate the oxidation and decay of precursors used in the experiments, ensuring that the correct amount of oxidant was accurately simulated. For all the photochemical experiments, the box model utilizing the USC-API mechanism was able to well-simulate the decay of α-pinene and NO for all experiments (Fig. 4-5). This comparison indicates that the developed mechanism well represents the oxidation of α-pinene and formation of oxidants under

https://doi.org/10.5194/egusphere-2024-3860
Preprint. Discussion started: 17 December 2024

a wide range of experimental conditions. The simulations using the USC-API mechanism was a vast improvement compared to using the RACM2 or the MCM subset for α-pinene chemistry for simulating NO and α-pinene decay for the photochemical experiments (Exp. 1-5).

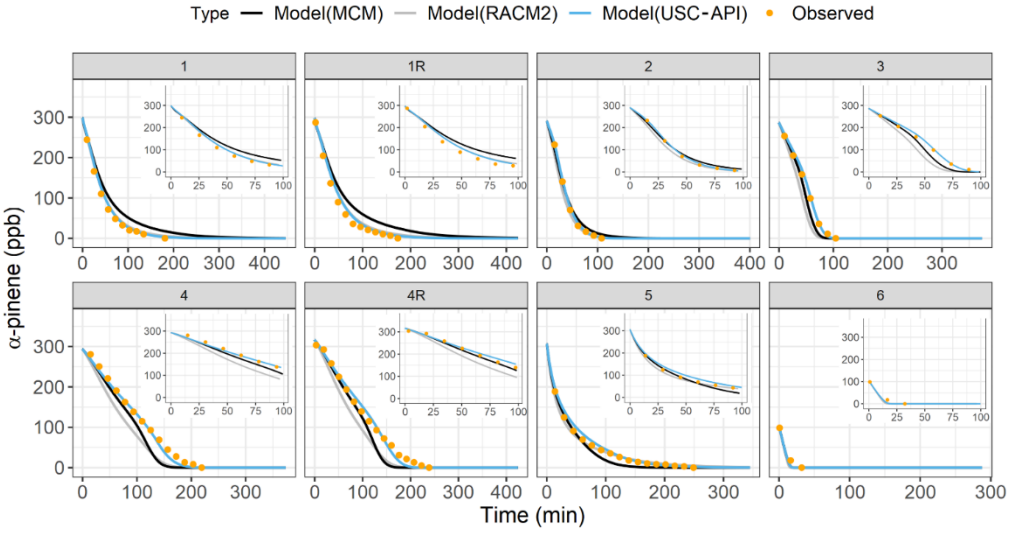

Fig. 4. The observed (orange data points) and the modeled (lines) α-pinene decay for the various conducted experiments. The modeled results are based on three chemical mechanisms: MCM (black), RACM2 (grey), and USC-API (light blue). Insets highlight the initial decay period from 0 to 100 minutes.

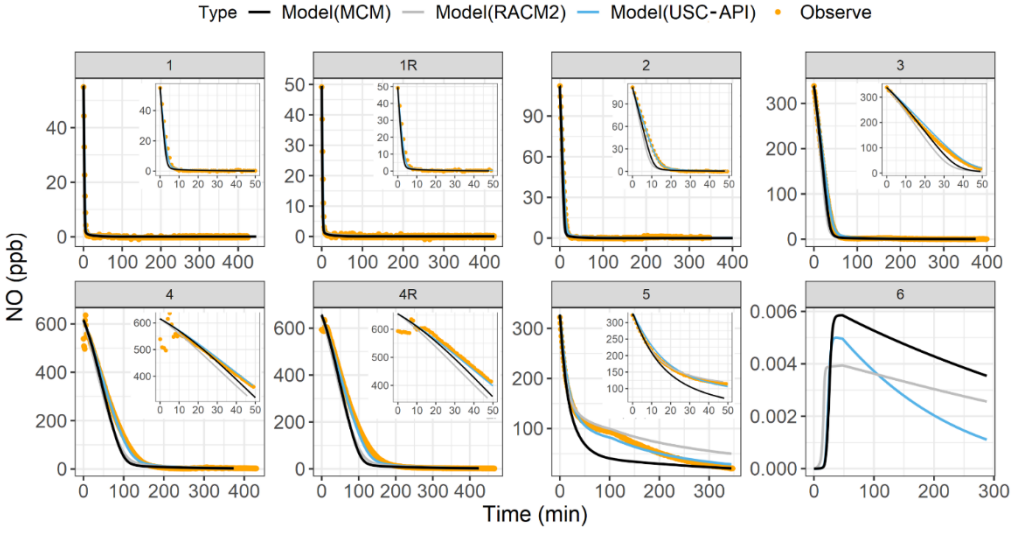

Fig. 5. The observed (orange data points) and the modeled (lines) NO decay for the various conducted experiments. The NO observations for Experiment 6 were not available. The modeled results are based on three chemical mechanisms: MCM (black), RACM2 (grey), and USC_API (light blue). Insets highlight the initial decay period from 0 to 50 minutes.

https://doi.org/10.5194/egusphere-2024-3860
Preprint. Discussion started: 17 December 2024

3.3.2 $\Delta^{17}O$ Simulation

The model simulations for the photochemical experiments indicate a substantial temporal change in $\Delta^{17}O(NO_2)$ (Fig. 6). The $\Delta^{17}O(NO_2)$ initially starts at 0‰ and begins to increase due to the production of O_3 that elevate $\Delta^{17}O(NO_2)$ as NO is oxidized by O_3. For the nighttime experiment, the box model predicts $\Delta^{17}O(NO_2)$ to remain steady with a value near 7.6‰, due to N_2O_5 thermal equilibrium with NO_2 and NO_3 resulting in the $\Delta^{17}O(NO_2) = \Delta^{17}O(N_2O_5)$. Generally, the $\Delta^{17}O$ simulation of NO_2 were in excellent agreement with the observations, as indicated by an RMSE of 1.7‰ (Table 3). Considering the range of observed $\Delta^{17}O(NO_2)$ values that spanned 34.2‰, the model RMSE value is quite exceptional. This strong agreement indicates that the box model and employed chemical mechanism well-represented the NO_x photochemical cycling and $NO_2/NO_3/N_2O_5$ thermal equilibrium. Further, our model analysis would indicate that an assumed $\Delta^{17}O(O_3^{term})$ value of 39‰, well-simulated the $\Delta^{17}O(NO_2)$ values across a range of experimental conditions. The strong agreement between the model and observations supports the robustness of our chemical mechanism in representing the critical oxidation processes and isotope transfer within the NO_x system. Additionally, the model's capability to simulate $\Delta^{17}O(NO_2)$ under both photochemical and nighttime conditions highlights its effectiveness in capturing the transition between photochemical and thermal equilibrium pathways in NO_x chemistry. For the nighttime experiment, the steady $\Delta^{17}O(NO_2)$ further confirms the model's accurate depiction of the equilibrium between NO_2, NO_3, and N_2O_5, an essential aspect of nighttime NO_x processing. This result indicates that the model is well-suited to describe isotope dynamics in environments with varying NO_x levels and oxidant influences.

The simulated $\Delta^{17}O(pNO_3)$ using the base mechanism closely matched the observations with an average RMSE of 1.2‰, indicating that the relative production routes of organic nitrate (+OH/O_2/NO vs +NO_3) were correctly simulated for the various experimental conditions (Fig. 7). Oxygen isotope mass-balance indicates that the α-pinene-derived peroxy radicals + NO pathway would be the expected pathway leaded to a low $\Delta^{17}O(pNO_3)$ value as only one oxygen atom in the nitro group of the generated $RONO_2$ could derive from O_3. In contrast, the *α*-pinene oxidation involving NO_3 leading to organic nitrate would be the pathway leading to a high $\Delta^{17}O(pNO_3)$ value as all of the oxygen atoms in the NO_3 group could derive from O_3 (Walters et al., 2024a). The excellent agreement between model and observation indicates that the developed chemical mechanism generally well-reproduced organic nitrate formation pathways involving *α*-pinene for the conducted photochemical experiments. Overall, the excellent agreement between model and observation for $\Delta^{17}O(pNO_3)$ provides confidence in the model's representation of organic nitrate formation involving *α*-pinene across diverse photochemical conditions. It suggests that the model's parameterization of *α*-pinene oxidation pathways and the resulting isotope fractionation effects on pNO_3 is well-calibrated, supporting its utility for simulating organic nitrate formation and its impact on aerosol chemistry.

The simulated $\Delta^{17}O$ of HNO_3 (Fig. 8) begins at 26‰, reflecting the assumed $\Delta^{17}O$ value of an HNO_3 chamber blank. This initial value was not directly measured but was estimated to achieve agreement with the measured $\Delta^{17}O$ of HNO_3 in Exp. 1 and Exp. 2, where HNO_3 production was relatively low (Fig. S1). At the onset of the experiment, $\Delta^{17}O(HNO_3)$ decreases as

https://doi.org/10.5194/egusphere-2024-3860
Preprint. Discussion started: 17 December 2024

newly formed HNO_3, which has a $\Delta^{17}O$ lower than the chamber blank value, begins to dominate. For Exp. 1, 2, and 6, $\Delta^{17}O(HNO_3)$ continues to decrease over time, eventually reaching a plateau as HNO_3 production ceases. In contrast, for Exp. 3, 4, and 5, after an initial decline in $\Delta^{17}O(HNO_3)$, the values begin to rise. This increase is driven by the production of HNO_3 with higher $\Delta^{17}O$ values, resulting from elevated $\Delta^{17}O(NO_2)$ associated with the buildup of O_3. Overall, the simulated $\Delta^{17}O(HNO_3)$ is proportional to the maximum $\Delta^{17}O(NO_2)$, reflecting the dilution of $\Delta^{17}O(NO_2)$ in additional NO_y products due to the incorporation of O atoms from oxidants other than O_3. Overall, the model does a poor job of capturing $\Delta^{17}O(HNO_3)$ relative to observations, with an average RMSE of 4.6‰ compared to an observed range of 8.2‰. The model reasonably aligns with observations for the Exp. 1 and 2, where measurements were influenced by a chamber blank or HNO_3 carry-over effect, assumed to have a $\Delta^{17}O(HNO_3)$ value of 26‰. However, for the high initial NO_x concentration experiments (Exp. 3, 4, and 5), the simulated $\Delta^{17}O(HNO_3)$ was consistently too high. In the high HNO_3 production experiments (Exp. 4 and 5), the influence of a potential chamber HNO_3 blank was negligible due to the large amount of HNO_3 produced (Fig. S1). Here, the discrepancies between measured and modeled $\Delta^{17}O(HNO_3)$ suggest a missing or under-accounted HNO_3 production pathway. Based on oxygen isotope mass-balance expectations, we identified two potential pathways that could yield a lower $\Delta^{17}O(HNO_3)$ than the dominant NO_2+OH channel, which has a $\Delta^{17}O$ transfer factor of $(2/3)(\Delta^{17}O(NO_2))$ (Alexander et al., 2020). First, the NO + HO_2 reaction was considered as a possible source of low-$\Delta^{17}O(HNO_3)$, with a $\Delta^{17}O$ transfer factor of $(1/3)(\Delta^{17}O(NO))$ (Alexander et al., 2020). However, this reaction is unlikely to explain the model mismatch since HO_2 levels were low in Exp 5. Second, organic nitrate hydrolysis could be a possible source of low-$\Delta^{17}O$ HNO_3, especially if derived from +OH/NO reactions with a $\Delta^{17}O$ transfer factor of $(1/3)(\Delta^{17}O(NO))$ (Walters et al., 2024a). This source of HNO_3 would not be consistent with the $\delta^{15}N$ data of HNO_3 and pNO_3, which indicated large differences suggesting that these molecules were not related (Fig. 2). Still, to test this hypothesis, we conducted a sensitivity analysis allowing pinene hydroxyl-nitrate, pinene carbonyl nitrate, and pinene nitrooxy-hydroperoxide to hydrolyze with a lifetime of 2 hours (Table S3). We did not enable the dimer or pinene dinitrate to hydrolyze since these were dominant organic nitrate formed during nighttime oxidation, which we found minimal hydrolysis to occur from the filter extracts (Fig. 3). This modified simulation, "USC_API_Hydro," slightly improved the $\Delta^{17}O(HNO_3)$ agreement for Exp. 3, 4, and 5, reducing the average RMSE from 5.5‰ in the base model to 3.8‰ in the updated model (Table 3). However, for experiments with low-medium initial NO_x concentration (Exp. 1 and 2), organic nitrate hydrolysis resulted in a higher RMSE (6.3‰) compared to the base model (1.9‰). Organic nitrate hydrolysis had minimal impact on $\Delta^{17}O(NO_2)$ but did affect $\Delta^{17}O(pNO_3)$, particularly in high initial NO_x concentration experiments. Specifically, including this pathway decreased model performance for $\Delta^{17}O(pNO_3)$ in Exp. 3 and 4, though it improved the fit for Exp. 5. Overall, despite considering hydrolysis of organic nitrate to HNO_3, the simulated $\Delta^{17}O(HNO_3)$ for Exp. 4 and 5 remained too high to match observations and was not improved by decreasing the hydrolysis lifetime.

Therefore, based on our oxygen-isotope mass-balance framework, we were unable to identify a suitable missing or under-constrained HNO_3 production source in the model to explain the relatively low observed $\Delta^{17}O(HNO_3)$ in high-NO_y experiments. Thus, we speculate that the collected HNO_3 in high initial NO_x experiments (Exp. 4 and 5) may not fully represent

https://doi.org/10.5194/egusphere-2024-3860
Preprint. Discussion started: 17 December 2024

HNO_3 produced under experimental conditions. While we would not expect $\Delta^{17}O$ fractionation if HNO_3 were incompletely collected by the denuder system, our results may be biased toward HNO_3 produced earlier in the experiments when $\Delta^{17}O(HNO_3)$ is expected to be lower (Fig. 8). Although our collection method yielded consistent and precise $\Delta^{17}O(HNO_3)$ values across repeat experiments (Blum et al., 2023), the accuracy of these values remains uncertain. These findings suggest that an alternative HNO_3 collection method may be necessary to more accurately characterize $\Delta^{17}O(HNO_3)$ in chamber experiments.

Overall, the results of the $\Delta^{17}O$ model simulations offer detailed insights into the oxidation chemistry dynamics associated with NO_x and α-pinene under varied photochemical and nighttime conditions. The model effectively captured the oxidation dynamics associated with NO_2 photochemical cycling and nighttime equilibrium as well as captured the chemistry associated with organic nitrate formation. However, the model displayed limitations in simulating $\Delta^{17}O(HNO_3)$, particularly for experiments with high initial NO_x conditions where the observed values were lower than predicted. Sensitivity analyses suggested that inclusion of additional HNO_3 formation pathways such as organic nitrate hydrolysis could partially improve the model's accuracy though further refinement is necessary and suggesting a potential artifact associated with HNO_3 collection.

Table 3. Summary of the calculated average RMSE for the $\Delta^{17}O$ model simulations using the USC-API chemistry and inclusion of organic nitrate hydrolysis (USC-API-Hydro) mechanism.

	$\Delta^{17}O(NO_2)$ (‰)			$\Delta^{17}O(pNO_3)$ (‰)			$\Delta^{17}O(HNO_3)$ (‰)		
Exp	USC-API	USC-API-Hydro	*n*	USC-API	USC-API-Hydro	*n*	USC-API	USC-API-Hydro	*n*
1	1.1	0.9	1	0.6	3.1	1	1.4	7.0	1
1R	2.0	1.9	1	0.8	1.0	1	3.7	9.3	1
2	3.9	3.9	1	0.4	1.5	1	0.5	2.7	1
3	0.6	0.6	3	0.6	0.9	1	5.5	3.0	3
4	2.5	2.6	3	1.2	2.1	1	5.0	2.2	3
4R	3.1	3.1	4	0.8	2.7	1	7.8	5.0	4
5	1.2	1.1	4	7.1	5.7	1	5.6	3.5	4
6	0.3	0.3	3	NA	NA	1	3.1	3.7	3
AVG	**1.8**	**1.8**		**1.6**	**2.4**		**4.1**	**4.6**	

https://doi.org/10.5194/egusphere-2024-3860
Preprint. Discussion started: 17 December 2024

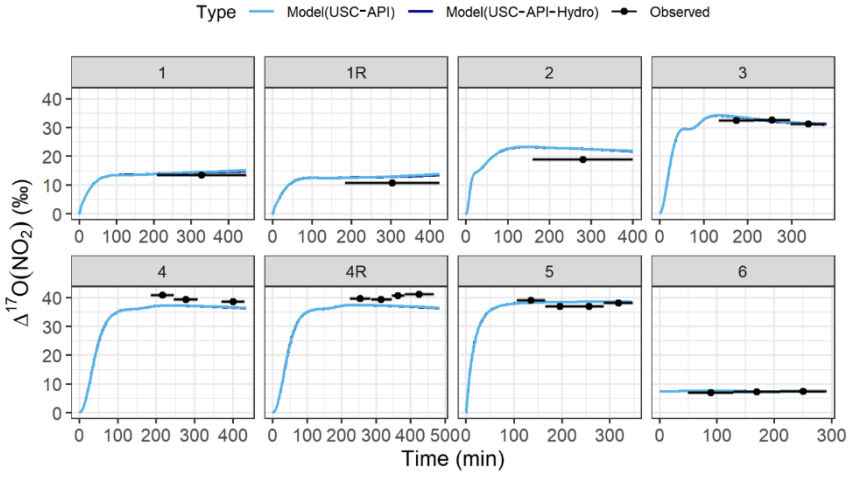

Fig. 6. Comparison between the modeled and observed $\Delta^{17}O(NO_2)$ values sorted by the various conducted experiments. The data points represent the average experiment time for each denuder collection, with the black line span the collection time range (from start to stop). The measurement uncertainty (±σ) is included as the lighter grey shaded region. The model simulations include both the base model (USC-API) and considering the potential role of organic nitrate hydrolysis (USC-API-Hydro). The inclusion of organic hydrolysis had a near negligible impact on $\Delta^{17}O(NO_2)$.

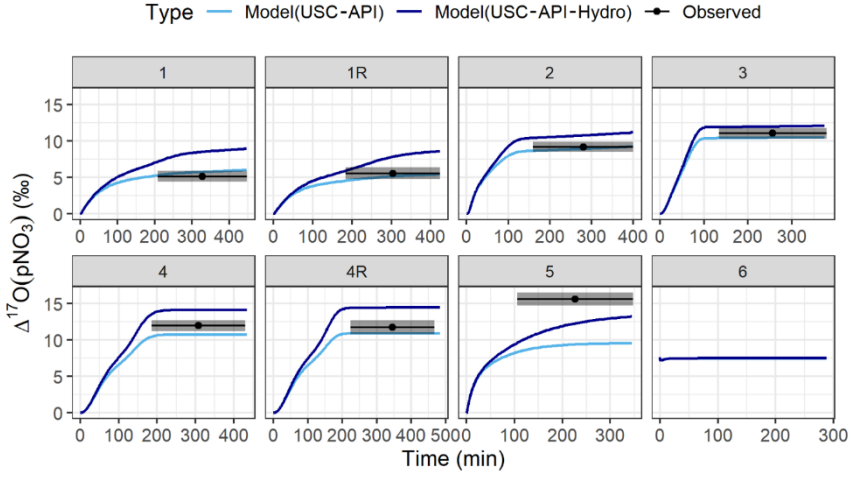

Fig. 7. Comparison between the modeled and observed $\Delta^{17}O(pNO_3)$ values sorted by the various conducted experiments. The data points represent the average experiment time for each denuder collection, with the black line span the collection time range (from start to stop). The measurement uncertainty (±σ) is included as the lighter grey shaded region. The model simulations include both the base model (USC-API) and considering the potential role of organic nitrate hydrolysis (USC-API-Hydro).

https://doi.org/10.5194/egusphere-2024-3860
Preprint. Discussion started: 17 December 2024

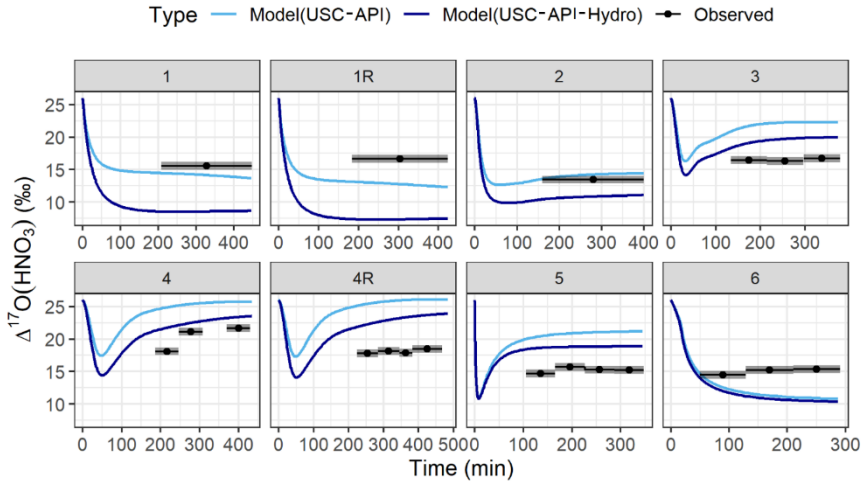

Fig. 8. Comparison between the modeled and observed $\Delta^{17}O(HNO_3)$ values sorted by the various conducted experiments. The data points represent the average experiment time for each denuder collection, with the black line span the collection time range (from start to stop). The measurement uncertainty (±σ) is included as the lighter grey shaded region. The model simulations include both the base model (USC-API) and considering the potential role of organic nitrate hydrolysis (USC-API-Hydro). The $\Delta^{17}O(HNO_3)$ is initially set at 26‰, based on the assumption that the HNO_3 "chamber blank" had this value.

3.3.3 $\delta^{15}N$ Simulation

The $\delta^{15}N$ simulations using the base chemistry mechanism indicate intriguing isotope dynamics (Fig. 9). Generally, the simulated $\delta^{15}N(NO_2)$ quickly increases at the start of the experiment due to the NO/NO_2 isotope exchange with a large isotope fractionation factor which preferentially favors the partitioning of ^{15}N into NO_2 relative to NO. For the photochemical experiments, as NO_2 is converted to HNO_3, the $\delta^{15}N(NO_2)$ decreases due to the assumed isotope fractionation associated with the NO_2 + OH reaction of 1.040 (Fang et al., 2021), favoring the preferential transfer of ^{15}N into the HNO_3 product. This also leads to the model predicting higher $\delta^{15}N(HNO_3)$ relative to NO_2, as the NO_2 + OH was the dominant reaction pathway for HNO_3 production in the photochemical experiments. The $\delta^{15}N(pNO_3)$ initially starts near the starting $\delta^{15}N(NO)$ value as α-pinene-derived peroxy radicals + NO was the main simulated formation pathway for the photochemical experiments. Due to the NO/NO_2 isotope equilibrium reaction, the $\delta^{15}N(NO)$ decreases relative to $\delta^{15}N(NO_x)$ as ^{15}N preferentially partitions into NO_2. This causes the low $\delta^{15}N$ of the formed pNO_3, which was derived from organic nitrate, relative to the other measured NO_y components.

Overall, the $\delta^{15}N(NO_2)$ simulation using the base chemistry model had decent agreement with the observations with an RMSE of 8.9‰; however, large disagreements were observed for photochemical experiments with elevated initial NO_y (Fig. 9; Table 4). For these experiments (Exp. 3-5), the simulated $\delta^{15}N(NO_2)$ were much lower than observed and the model predicted a

https://doi.org/10.5194/egusphere-2024-3860
Preprint. Discussion started: 17 December 2024

substantial decrease in $\delta^{15}N(NO_2)$ as the experiment progresses which was not observed. The photochemical cycling involving NO_x was well-simulated using the model chemistry as evidenced by a strong concentration and $\Delta^{17}O$ agreement between observations and model. It is inherently more challenging to model $\delta^{15}N$ compared to $\Delta^{17}O$ of NO_y compounds. This is due to mass-dependent fractionation that can have a significant impact on $\delta^{15}N$ values, which is largely assumed in the adapted i_NRACM mechanism (Fang et al., 2021). Therefore, we speculate that the $\delta^{15}N(NO_2)$ model disagreement could be due to inaccurate nitrogen fractionation utilized within i_NRACM. The model simulation predicted a substantial decrease in $\delta^{15}N(NO_2)$ as the experiments progressed due to the large nitrogen isotope fractionation factor or KIE associated with the NO_2 + OH reaction assumed in the i_NRACM mechanism to be 1.040 (Fang et al., 2021), defined as (Eq. 9):

$$KIE = {}^{15}\alpha = \frac{{}^{15}NO_2+OH}{{}^{14}NO_2+OH} \quad \text{(Eq. 9)}$$

Previously, the KIE associated with this reaction has been estimated to be 0.997 based on the reduced masses in the transition complex (Freyer, 1991). Therefore, we also conducted additional $\delta^{15}N$ simulations using a KIE (or $^{15}\alpha$) for the NO_2 + OH reaction of 0.997 (Fig. 6), noted as the USC-API-KIE. The modified $\delta^{15}N(NO_2)$ simulations, using the adjusted NO_2 + OH KIE, resulted in a better agreement with the observations decreasing the RMSE from 8.9 to 2.6 ‰ (Table 4). Considering the large range of $\delta^{15}N(NO_2)$ observations that spanned 72.2‰, the modified $\delta^{15}N(NO_2)$ simulations are in close agreement (within 4%) of the observations. Further, the modified simulations indicated that $\delta^{15}N(NO_2)$ temporal simulation better matched the observations for the photochemical experiments with high initial NO concentrations (Exp 3-5) (Fig. 9). Overall, based on a comparison of measured to simulated $\delta^{15}N(NO_2)$, the NO_2 + OH KIE was best approximated using a value of 0.997, enabling the accurate simulation of $\delta^{15}N(NO_2)$.

Generally, the simulated $\delta^{15}N(pNO_3)$ values were in close agreement with the observations with an RMSE of 5.0‰ for the base simulations (Fig. 10; Table 4), especially considered the measurement uncertainty that was as high as 4.1‰ due to a significant filter NO_3^- blank. The modified $\delta^{15}N$ simulations using the adjusted NO_2 + OH $^{15}\alpha$ of 0.997 slightly decreased the RMSE of $\delta^{15}N(pNO_3)$ to 4.5%. The simulated $\delta^{15}N(pNO_3)$ were insensitive to the adjustments for NO_2 + OH KIE because the organic nitrate formed relatively quickly under the experimental conditions before significant influence of the NO_2 + OH isotope effect on the residual $\delta^{15}N(NO_x)$. Overall, this excellent $\delta^{15}N$ comparison indicates that the adapted i_NRACM mechanism well-describes the fractionation associated with NO + α-pinene derived peroxy radicals. This result validates the mechanism's utility for modeling $\delta^{15}N$ values in similar organic-influenced photochemical environments.

In contrast to $\delta^{15}N(NO_2)$ and $\delta^{15}N(pNO_3)$, the model struggled to accurately simulate the $\delta^{15}N(HNO_3)$ observations with an RMSE of 12.5‰ for the base model simulation (Fig. 11; Table 4). The modified $\delta^{15}N$ simulations that included an update to NO_2 + OH $^{15}\alpha$ to 0.997, led to worse agreement between the model and observed $\delta^{15}N(HNO_3)$ values with an RMSE of 24.1‰. Notably, the modified $\delta^{15}N$ model mechanism simulations significantly improved the model $\delta^{15}N(HNO_3)$ agreement with observations for the HONO experiments, which were too high in the base model simulations (Fig. 11). However, the modified

https://doi.org/10.5194/egusphere-2024-3860
Preprint. Discussion started: 17 December 2024

630 mechanism led to a worse agreement between the simulated $\delta^{15}N(HNO_3)$ and observations for the photochemical experiments involving H_2O_2 and NO (Exp 1-4). We speculate that these differences could be due to sampling artifacts or HNO_3 loss on the chamber wall and/or sampling inlets, consistent with our findings for the $\Delta^{17}O(HNO_3)$ simulations. These artifacts highlight the challenges associated with accurately capturing $\delta^{15}N(HNO_3)$ in chamber studies, where wall effects and sampling techniques may interfere with precise isotopic measurements.

635

Our model comparison highlights the complexity of simulating nitrogen isotope dynamics in atmospheric chamber experiments. The improved $\delta^{15}N(NO_2)$ agreement with an adjusted KIE value for NO_2 + OH highlights the sensitivity of nitrogen isotopes to specific fractionation processes. While $\delta^{15}N(pNO_3)$ simulations were robust to changes in KIE, indicating the stability of iNRACM's treatment of NO + organic peroxy radical interactions, the $\delta^{15}N(HNO_3)$ simulations revealed
640 limitations in both base and modified models. The findings suggest that additional factors, such as chamber wall interactions, may need to be considered to improve $\delta^{15}N(HNO_3)$ model performance. Future studies should prioritize refining isotopic fractionation factors, especially for reactions involving reactive nitrogen oxides and hydroxyl radicals, to better capture nitrogen isotope variability in photochemical environments. Additionally, advancements in experimental setups to mitigate sampling artifacts could enhance the reliability of $\delta^{15}N$ measurements, thereby improving model accuracy for nitrogen isotopic
645 compositions in complex photochemical systems.

Table 4. Summary of the calculated average RMSE for the $\delta^{15}N$ model simulations using the base chemistry (USC-API) and the KIE mechanism (USC-API-KIE), which includes an updated $^{15}\alpha$ for the NO_2+OH reaction of 0.997.

	$\delta^{15}N(NO_2)$ (‰)			$\delta^{15}N(pNO_3)$ (‰)			$\delta^{15}N(HNO_3)$ (‰)		
Exp	USC-API	USC-API-KIE	*n*	USC-API	USC-API-KIE	*n*	USC-API	USC-API-KIE	*n*
1	5.8	0.7	1	1.1	3.2	1	2.0	18.5	1
1R	9.4	3.7	1	2.0	0.1	1	1.1	18.9	1
2	6.1	1.9	1	3.7	0.9	1	5.2	29.5	1
3	15.0	1.6	3	14.9	12.7	1	19.1	44.2	3
4	11.3	1.8	3	4.1	5.9	1	7.8	23.6	3
4R	15.7	2.5	4	0.0	1.7	1	8.1	37.9	4
5	3.0	4.0	4	9.2	6.8	1	38.8	2.2	4
6	4.8	4.8	3	N/A	N/A	1	18.0	18.1	3
AVG	**8.9**	**2.6**		**5.0**	**4.5**		**12.5**	**24.1**	

https://doi.org/10.5194/egusphere-2024-3860
Preprint. Discussion started: 17 December 2024

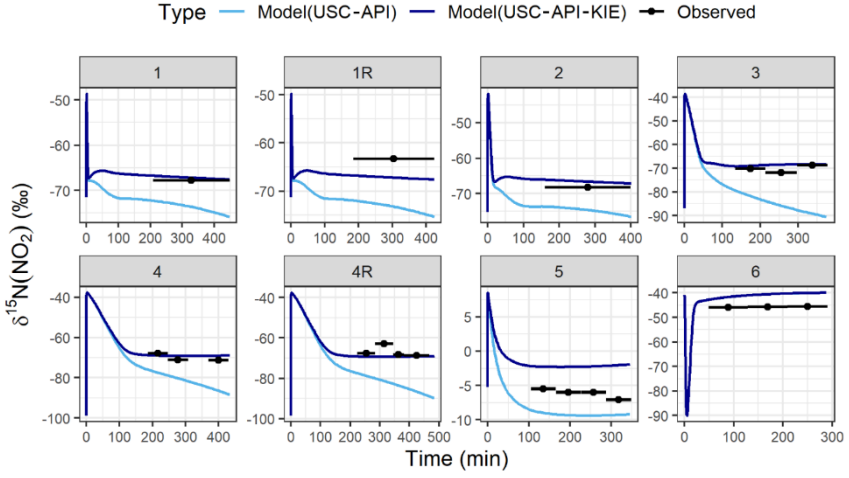

Fig. 9. Comparison between the modeled and observed $\delta^{15}N(NO_2)$ values sorted by the various conducted experiments. The data points represent the average experiment time for each denuder collection, with the black line span the collection time range (from start to stop). The model simulations include both the base model (USC-API) and an update to the NO_2 + OH nitrogen isotope fractionation factor ($^{15}\alpha$ = 0.997) (USC-API-KIE) as opposed to the base model with $^{15}\alpha$ = 1.040. For Exp. 6, a nighttime experiment, the $\delta^{15}N$ simulation using USC-API and USC-API-KIE were similar due to the limited role of the NO_2+OH reaction under those conditions.

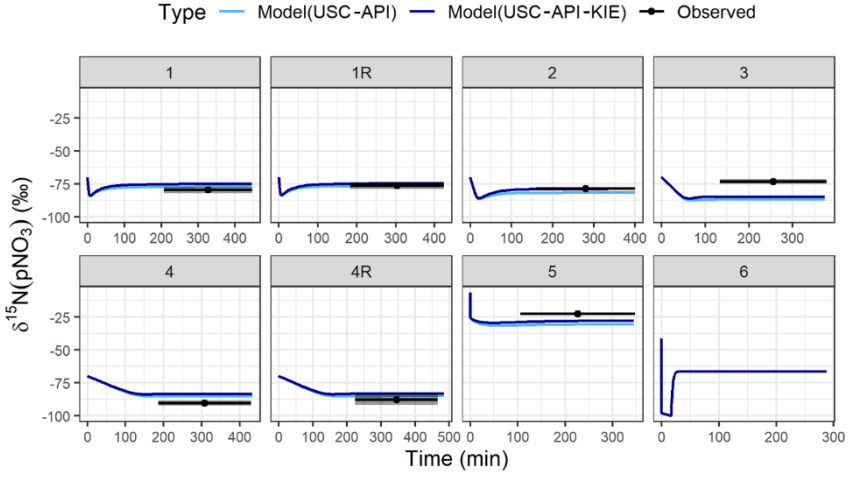

Fig. 10. Comparison between the modeled and observed $\delta^{15}N(pNO_3)$ values sorted by the various conducted experiments. The data points represent the average experiment time for each denuder collection, with the black line span the collection time range (from start to stop). The model simulations include both the base model (USC-API) and an update to the NO_2 + OH nitrogen isotope fractionation factor ($^{15}\alpha$ = 0.997) (USC-API-KIE) as opposed to the base model with $^{15}\alpha$ = 1.040. For Exp. 6, a nighttime experiment, the $\delta^{15}N$ simulation using USC-API and USC-API-KIE were similar due to the limited role of the NO_2+OH reaction under those conditions.

https://doi.org/10.5194/egusphere-2024-3860
Preprint. Discussion started: 17 December 2024

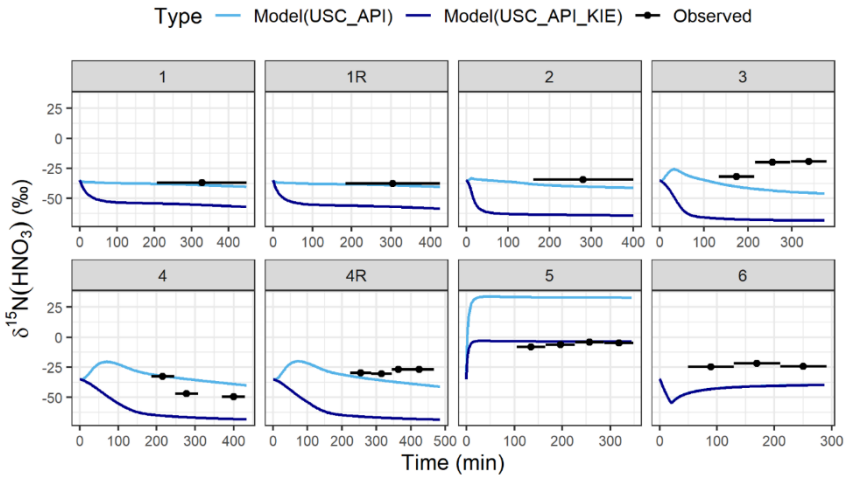

Fig. 11. Comparison between the modeled and observed $\delta^{15}N(HNO_3)$ values sorted by the various conducted experiments. The data points represent the average experiment time for each denuder collection, with the black line span the collection time range (from start to stop). The model simulations include both the base model (USC-API) and an update to the NO_2 + OH nitrogen isotope fractionation factor ($^{15}\alpha$ = 0.997) (USC-API-KIE) as opposed to the base model with $^{15}\alpha$ = 1.040. For Exp. 6, a nighttime experiment, the $\delta^{15}N$ simulation using USC-API and USC-API-KIE were similar due to the limited role of the NO_2+OH reaction under those conditions.

5. Conclusion

This study provides a comprehensive investigation of NO_x and BVOC oxidation chemistry using stable isotope analyses and chemical modeling. Through $\Delta^{17}O$ and $\delta^{15}N$ observations compared to model simulation, we gained critical insights into $\Delta^{17}O$ transfer dynamics involved NO_x oxidation chemistry and nitrogen isotope fractionation. By adopting a $\Delta^{17}O$ value for O_3^{term} of 39‰, our model utilizing a recently developed $\Delta^{17}O$ transfer framework successfully reproduced $\Delta^{17}O$ values for NO_2 across diverse environmental conditions, affirming the robustness of the photochemical understanding of $\Delta^{17}O$ transfer dynamics. Furthermore, under the experimental conditions, we derived a $\delta^{18}O$ value of 106±5‰ for oxygen atoms transferred into NO_y from the O_3^{term}, and a value of 11.8±1.0‰ for oxygen atoms transferred from other oxidants, such as RO_2, HO_2, and OH. Moreover, we found that the recently developed I_NRACM model framework for simulating $\delta^{15}N$ was significantly improved by adopting a $^{15}\alpha$ = 0.997 for the NO_2+OH reaction, leading to better agreement with $\delta^{15}N(NO_2)$. This result highlights the importance of refining fractionation assumptions in isotope-based chemical mechanisms. However, the updated fractionation factor introduced challenges in accurately simulating $\delta^{15}N$ values for HNO_3, highlighting persistent uncertainties in the sampling and modeling of HNO_3 under the experimental conditions.

https://doi.org/10.5194/egusphere-2024-3860
Preprint. Discussion started: 17 December 2024

Our development of the USC-API mechanism marked a substantial advancement over existing frameworks such as RACM2 and MCM for describing NO_x and BVOC oxidation. This mechanism not only captured NO_x photochemical cycling and α-pinene decay dynamics but also provided accurate simulations of organic nitrate production. One of the major implications of this mechanism is that the weighted branching ratio of α-pinene+OH+NO leading to organic nitrate versus NO_2 production was set to 0.222 based on the MCM, which led to the correct photochemical dynamics involving NO_x, which was evaluated using $\Delta^{17}O$. The mechanism further clarified the roles of daytime α-pinene+OH+NO reactions versus nighttime α-pinene+NO_3 reactions contributing to organic nitrate production. Our model and result comparisons indicate instances where the α-pinene+NO_3+ HO_2 pathway significantly contributed to organic nitrate production during photochemical experiments. This nuanced understanding of organic nitrate formation has implications for atmospheric NO_x budgets and SOA production.

Isotope observations and model simulation revealed stark differences between HNO_3 (medium-high $\Delta^{17}O$ and high $\delta^{15}N$) and particulate nitrate (pNO_3; low $\Delta^{17}O$ and low $\delta^{15}N$), indicating distinct formation pathways. Our findings strongly suggest that pNO_3 in these experiments originated exclusively from organic nitrate, a conclusion supported by online AMS data. Furthermore, the $\Delta^{17}O$ and $\delta^{15}N$ evidence demonstrated that organic nitrate hydrolysis was not a major source of HNO_3 under the studied conditions, which predominantly involved low relative humidity. These insights offer new opportunities to probe pNO_3 hydrolysis and its implications for nitrate chemistry under varying environmental conditions. Despite these advances, limitations in accurately modeling $\Delta^{17}O$ and $\delta^{15}N$ values for HNO_3 highlighting the need for improved collection methodologies. Experimental artifacts, potentially linked to the use of long sampling lines and HNO_3 losses in chamber experiments, may have biased the collected data. These methodological challenges indicate the importance of refining sampling techniques for HNO_3 in chamber experiments to ensure representative measurements in future studies.

The implications of this work extend beyond the laboratory setting. Stable isotope techniques demonstrated their potential as powerful tools for probing complex NO_x and BVOC interactions and atmospheric oxidation chemistry. Future research should aim to expand these methodologies to other BVOC systems under a wider array of conditions, including variations in relative humidity, aerosol seed composition, and oxidant availability. Furthermore, integrating isotope techniques into field campaigns could provide invaluable constraints on NO_x oxidation and organic nitrate formation processes in real-world atmospheric environments. Overall, this study not only advances our understanding of the oxygen and nitrogen stable isotope dynamics involved in NO_x oxidation chemistry, but also provide insights into NO_x and BVOC chemistry. Addressing the limitations identified here and applying these techniques across broader contexts will enhance the predictive power of atmospheric chemistry models, aiding in the development of more effective air quality management strategies and climate policies.

Code and Data availability. The box model simulations, including model mechanisms, input files, and output files have been made publicly available at: https://zenodo.org/records/14241585. The experimental data and figure codes have been made

https://doi.org/10.5194/egusphere-2024-3860
Preprint. Discussion started: 17 December 2024

publicly available at: https://zenodo.org/records/14241591. The chemical mechanism and isotope data are provided in the Supplementary Material.

Author contributions. WWW, MT, NLN, MGH designed the conducted experiments. WWW, MT, DEB, GE, PT, WX, JR, FL, GH, JBM conducted the experiments. WWW and DEB conducted the offline data analysis. WWW conducted the chamber simulations with input from MGH, MT and NLN. WWW wrote the manuscript with input from all authors. WWW and MGH secured funding.

Competing interests. The contact author has declared that none of the authors has any competing interests.

Acknowledgements. We thank Ruby Ho for laboratory assistance.

Financial Support. This research has been supported by NOAA's Climate Program Office's Atmospheric Chemistry, Carbon Cycle, and Climate Program (NOAA AC4 NA18OAR4310118).

References

Albertin, S., Savarino, J., Bekki, S., Barbero, A., and Caillon, N.: Measurement report: Nitrogen isotopes ($\delta^{15}N$) and first quantification of oxygen isotope anomalies ($\Delta^{17}O$, $\delta^{18}O$) in atmospheric nitrogen dioxide, Atmospheric Chemistry and Physics, 21, 10477–10497, https://doi.org/10.5194/acp-21-10477-2021, 2021.

Alexander, B., Sherwen, T., Holmes, C. D., Fisher, J. A., Chen, Q., Evans, M. J., and Kasibhatla, P.: Global inorganic nitrate production mechanisms: comparison of a global model with nitrate isotope observations, Atmospheric Chemistry and Physics, 20, 3859–3877, https://doi.org/10.5194/acp-20-3859-2020, 2020.

Aschmann, S. M., Atkinson, R., and Arey, J.: Products of reaction of OH radicals with α-pinene, J.-Geophys.-Res., 107, https://doi.org/10.1029/2001JD001098, 2002.

Bates, K. H., Burke, G. J., Cope, J. D., and Nguyen, T. B.: Secondary organic aerosol and organic nitrogen yields from the nitrate radical (NO3) oxidation of alpha-pinene from various RO2 fates, Atmospheric Chemistry and Physics, 22, 1467–1482, https://doi.org/10.5194/acp-22-1467-2022, 2022.

Beaver, M. R., Clair, J. S., Paulot, F., Spencer, K. M., Crounse, J. D., LaFranchi, B. W., Min, K. E., Pusede, S. E., Wooldridge, P. J., and Schade, G. W.: Importance of biogenic precursors to the budget of organic nitrates: observations of multifunctional organic nitrates by CIMS and TD-LIF during BEARPEX 2009, Atmospheric Chemistry and Physics, 12, 5773–5785, https://doi.org/10.5194/acp-12-5773-2012, 2012.

https://doi.org/10.5194/egusphere-2024-3860
Preprint. Discussion started: 17 December 2024

Bekker, C., Walters, W. W., Murray, L. T., and Hastings, M. G.: Nitrate chemistry in the northeast US – Part 1: Nitrogen isotope seasonality tracks nitrate formation chemistry, Atmospheric Chemistry and Physics, 23, 4185–4201, https://doi.org/10.5194/acp-23-4185-2023, 2023.

Bell, D. M., Wu, C., Bertrand, A., Graham, E., Schoonbaert, J., Giannoukos, S., Baltensperger, U., Prevot, A. S. H., Riipinen, I., El Haddad, I., and Mohr, C.: Particle-phase processing of α-pinene NO_3 secondary organic aerosol in the dark, Atmospheric Chemistry and Physics, 22, 13167–13182, https://doi.org/10.5194/acp-22-13167-2022, 2022.

Blum, D. E., Walters, W. W., and Hastings, M. G.: Speciated Collection of Nitric Acid and Fine Particulate Nitrate for Nitrogen and Oxygen Stable Isotope Determination, Anal. Chem., 92, 16079–16088, https://doi.org/10.1021/acs.analchem.0c03696, 2020.

Blum, D. E., Walters, W. W., Eris, G., Takeuchi, M., Huey, L. G., Tanner, D., Xu, W., Rivera-Rios, J. C., Liu, F., Ng, N. L., and Hastings, M. G.: Collection of Nitrogen Dioxide for Nitrogen and Oxygen Isotope Determination─Laboratory and Environmental Chamber Evaluation, Anal. Chem., 95, 3371–3378, https://doi.org/10.1021/acs.analchem.2c04672, 2023.

Böhlke, J. K., Mroczkowski, S. J., and Coplen, T. B.: Oxygen isotopes in nitrate: New reference materials for 18O: 17O: 16O measurements and observations on nitrate-water equilibration, Rapid Communications in Mass Spectrometry, 17, 1835–1846, https://doi.org/10.1002/rcm.1123, 2003.

Böhlke, J. K., Smith, R. L., and Hannon, J. E.: Isotopic analysis of N and O in nitrite and nitrate by sequential selective bacterial reduction to N2O, Analytical chemistry, 79, 5888–5895, https://doi.org/10.1021/ac070176k, 2007.

Boyd, C. M., Sanchez, J., Xu, L., Eugene, A. J., Nah, T., Tuet, W. Y., Guzman, M. I., and Ng, N. L.: Secondary organic aerosol formation from the β-pinene+ NO 3 system: effect of humidity and peroxy radical fate, Atmospheric Chemistry and Physics, 15, 7497–7522, https://doi.org/10.5194/acp-15-7497-2015, 2015.

Browne, E. C. and Cohen, R. C.: Effects of biogenic nitrate chemistry on the NO_x lifetime in remote continental regions, Atmospheric Chemistry and Physics, 12, 11917–11932, https://doi.org/10.5194/acp-12-11917-2012, 2012.

Browne, E. C., Wooldridge, P. J., Min, K.-E., and Cohen, R. C.: On the role of monoterpene chemistry in the remote continental boundary layer, Atmospheric Chemistry and Physics, 14, 1225–1238, https://doi.org/10.5194/acp-14-1225-2014, 2014.

Casciotti, K. L., Sigman, D. M., Hastings, M. G., Böhlke, J. K., and Hilkert, A.: Measurement of the oxygen isotopic composition of nitrate in seawater and freshwater using the denitrifier method, Analytical Chemistry, 74, 4905–4912, https://doi.org/10.1021/ac020113w, 2002.

Chai, J. and Hastings, M. G.: Collection Method for Isotopic Analysis of Gaseous Nitrous Acid, Anal. Chem., 90, 830–838, https://doi.org/10.1021/acs.analchem.7b03561, 2018.

https://doi.org/10.5194/egusphere-2024-3860
Preprint. Discussion started: 17 December 2024

Craig, H.: Isotopic standards for carbon and oxygen and correction factors for mass-spectrometric analysis of carbon dioxide, Geochimica et Cosmochimica Acta, 12, 133–149, https://doi.org/10.1016/0016-7037(57)90024-8, 1957.

Day, D. A., Liu, S., Russell, L. M., and Ziemann, P. J.: Organonitrate group concentrations in submicron particles with high nitrate and organic fractions in coastal southern California, Atmospheric Environment, 44, 1970–1979, https://doi.org/10.1016/j.atmosenv.2010.02.045, 2010.

DeCarlo, P. F., Kimmel, J. R., Trimborn, A., Northway, M. J., Jayne, J. T., Aiken, A. C., Gonin, M., Fuhrer, K., Horvath, T., and Docherty, K. S.: Field-deployable, high-resolution, time-of-flight aerosol mass spectrometer, Analytical chemistry, 78, 8281–8289, https://doi.org/10.1021/ac061249n, 2006.

Elliott, E. M., Yu, Z., Cole, A. S., and Coughlin, J. G.: Isotopic advances in understanding reactive nitrogen deposition and atmospheric processing, Science of The Total Environment, 662, 393–403, https://doi.org/10.1016/j.scitotenv.2018.12.177, 2019.

Fang, H., Walters, W. W., Mase, D., and Michalski, G.: i_NRACM: incorporating ^{15}N into the Regional Atmospheric Chemistry Mechanism (RACM) for assessing the role photochemistry plays in controlling the isotopic composition of NO_x, NO_y, and atmospheric nitrate, Geoscientific Model Development, 14, 5001–5022, https://doi.org/10.5194/gmd-14-5001-2021, 2021.

Farmer, D. K., Matsunaga, A., Docherty, K. S., Surratt, J. D., Seinfeld, J. H., Ziemann, P. J., and Jimenez, J. L.: Response of an aerosol mass spectrometer to organonitrates and organosulfates and implications for atmospheric chemistry, Proceedings of the National Academy of Sciences, 107, 6670–6675, https://doi.org/10.1073/pnas.0912340107, 2010.

Fibiger, D. L., Hastings, M. G., Lew, A. F., and Peltier, R. E.: Collection of NO and NO2 for Isotopic Analysis of NOx Emissions, Anal. Chem., 86, 12115–12121, https://doi.org/10.1021/ac502968e, 2014.

Fisher, J. A., Jacob, D. J., Travis, K. R., Kim, P. S., Marais, E. A., Chan Miller, C., Yu, K., Zhu, L., Yantosca, R. M., Sulprizio, M. P., Mao, J., Wennberg, P. O., Crounse, J. D., Teng, A. P., Nguyen, T. B., St. Clair, J. M., Cohen, R. C., Romer, P., Nault, B. A., Wooldridge, P. J., Jimenez, J. L., Campuzano-Jost, P., Day, D. A., Hu, W., Shepson, P. B., Xiong, F., Blake, D. R., Goldstein, A. H., Misztal, P. K., Hanisco, T. F., Wolfe, G. M., Ryerson, T. B., Wisthaler, A., and Mikoviny, T.: Organic nitrate chemistry and its implications for nitrogen budgets in an isoprene- and monoterpene-rich atmosphere: constraints from aircraft (SEAC^{4}RS) and ground-based (SOAS) observations in the Southeast US, Atmospheric Chemistry and Physics, 16, 5969–5991, https://doi.org/10.5194/acp-16-5969-2016, 2016.

Freyer, H. D.: Seasonal variation of 15N/14N ratios in atmospheric nitrate species, Tellus B, 43, 30–44, https://doi.org/10.3402/tellusb.v43i1.15244, 1991.

Freyer, H. D., Kley, D., Volz-Thomas, A., and Kobel, K.: On the interaction of isotopic exchange processes with photochemical reactions in atmospheric oxides of nitrogen, Journal of Geophysical Research, 98, 14791–14796, https://doi.org/10.1029/93JD00874, 1993.

https://doi.org/10.5194/egusphere-2024-3860
Preprint. Discussion started: 17 December 2024

Fry, J. L., Kiendler-Scharr, A., Rollins, A. W., Wooldridge, P. J., Brown, S. S., Fuchs, H., Dubé, W., Mensah, A., Dal Maso, M., and Tillmann, R.: Organic nitrate and secondary organic aerosol yield from NO 3 oxidation of β-pinene evaluated using a gas-phase kinetics/aerosol partitioning model, Atmospheric Chemistry and Physics, 9, 1431–1449, https://doi.org/10.5194/acp-9-1431-2009, 2009.

Fry, J. L., Draper, D. C., Barsanti, K. C., Smith, J. N., Ortega, J., Winkler, P. M., Lawler, M. J., Brown, S. S., Edwards, P. M., Cohen, R. C., and Lee, L.: Secondary Organic Aerosol Formation and Organic Nitrate Yield from NO3 Oxidation of Biogenic Hydrocarbons, Environ. Sci. Technol., 48, 11944–11953, https://doi.org/10.1021/es502204x, 2014.

Goliff, W. S., Stockwell, W. R., and Lawson, C. V.: The regional atmospheric chemistry mechanism, version 2, Atmospheric Environment, 68, 174–185, https://doi.org/10.1016/j.atmosenv.2012.11.038, 2013.

Hallquist, M., Wängberg, I., Ljungström, E., Barnes, I., and Becker, K.-H.: Aerosol and Product Yields from NO_3 Radical-Initiated Oxidation of Selected Monoterpenes, Environ. Sci. Technol., 33, 553–559, https://doi.org/10.1021/es980292s, 1999.

Hastings, M. G., Sigman, D. M., and Lipschultz, F.: Isotopic evidence for source changes of nitrate in rain at Bermuda, Journal of Geophysical Research: Atmospheres, 108, https://doi.org/10.1029/2003JD003789, 2003.

Hastings, M. G., Casciotti, K. L., and Elliott, E. M.: Stable isotopes as tracers of anthropogenic nitrogen sources, deposition, and impacts, Elements, 9, 339–344, https://doi.org/10.2113/gselements.9.5.339, 2013.

Hoyle, C. R., Boy, M., Donahue, N. M., Fry, J. L., Glasius, M., Guenther, A., Hallar, A. G., Huff Hartz, K., Petters, M. D., and Petäjä, T.: A review of the anthropogenic influence on biogenic secondary organic aerosol, Atmospheric Chemistry and Physics, 11, 321–343, https://doi.org/10.5194/acp-11-321-2011, 2011.

Huey, L. G., Dunlea, E. J., Lovejoy, E. R., Hanson, D. R., Norton, R. B., Fehsenfeld, F. C., and Howard, C. J.: Fast time response measurements of HNO3 in air with a chemical ionization mass spectrometer, Journal of Geophysical Research: Atmospheres, 103, 3355–3360, 1998.

Ishino, S., Hattori, S., Savarino, J., Jourdain, B., Preunkert, S., Legrand, M., Caillon, N., Barbero, A., Kuribayashi, K., and Yoshida, N.: Seasonal variations of triple oxygen isotopic compositions of atmospheric sulfate, nitrate, and ozone at Dumont d'Urville, coastal Antarctica, Atmos. Chem. Phys., 17, 3713–3727, https://doi.org/10.5194/acp-17-3713-2017, 2017.

Jenkin, M. E., Saunders, S. M., and Pilling, M. J.: The tropospheric degradation of volatile organic compounds: a protocol for mechanism development, Atmospheric Environment, 31, 81–104, https://doi.org/10.1016/S1352-2310(96)00105-7, 1997.

Kiendler-Scharr, A., Mensah, A. A., Friese, E., Topping, D., Nemitz, E., Prévôt, A. S., Äijälä, M., Allan, J., Canonaco, F., and Canagaratna, M.: Ubiquity of organic nitrates from nighttime chemistry in the European submicron aerosol, Geophysical research letters, 43, 7735–7744, https://doi.org/10.1002/2016GL069239, 2016.

https://doi.org/10.5194/egusphere-2024-3860
Preprint. Discussion started: 17 December 2024

Kim, H., Walters, W. W., Bekker, C., Murray, L. T., and Hastings, M. G.: Nitrate Chemistry in the Northeast US Part II: Oxygen Isotopes Reveal Differences in Particulate and Gas Phase Formation, Atmospheric Chemistry and Physics Discussions, 2022, 1–33, https://doi.org/10.5194/acp-2022-622, 2022.

Kroll, J. H., Ng, N. L., Murphy, S. M., Flagan, R. C., and Seinfeld, J. H.: Secondary organic aerosol formation from isoprene photooxidation under high-NOx conditions, Geophysical Research Letters, 32, https://doi.org/10.1021/es0524301, 2005.

Li, J., Zhang, X., Orlando, J., Tyndall, G., and Michalski, G.: Quantifying the nitrogen isotope effects during photochemical equilibrium between NO and NO_2: implications for $\delta^{15}N$ in tropospheric reactive nitrogen, Atmospheric Chemistry and Physics, 20, 9805–9819, https://doi.org/10.5194/acp-20-9805-2020, 2020.

Li, J., Davy, P., Harvey, M., Katzman, T., Mitchell, T., and Michalski, G.: Nitrogen isotopes in nitrate aerosols collected in the remote marine boundary layer: Implications for nitrogen isotopic fractionations among atmospheric reactive nitrogen species, Atmospheric Environment, 245, 118028, https://doi.org/10.1016/j.atmosenv.2020.118028, 2021.

Lopez-Hilfiker, F. D., Mohr, C., Ehn, M., Rubach, F., Kleist, E., Wildt, J., Mentel, T. F., Lutz, A., Hallquist, M., and Worsnop, D.: A novel method for online analysis of gas and particle composition: description and evaluation of a Filter Inlet for Gases and AEROsols (FIGAERO), Atmospheric Measurement Techniques, 7, 983–1001, https://doi.org/10.5194/amt-7-983-2014, 2014.

Lyons, J. R.: Transfer of mass-independent fractionation in ozone to other oxygen-containing radicals in the atmosphere, Geophysical Research Letters, 28, 3231–3234, 2001.

McIlvin, M. R. and Altabet, M. A.: Chemical Conversion of Nitrate and Nitrite to Nitrous Oxide for Nitrogen and Oxygen Isotopic Analysis in Freshwater and Seawater, Anal. Chem., 77, 5589–5595, https://doi.org/10.1021/ac050528s, 2005.

Michalski, G., Scott, Z., Kabiling, M., and Thiemens, M. H.: First measurements and modeling of Δ17O in atmospheric nitrate, Geophys. Res. Lett., 30, 1870, https://doi.org/10.1029/2003GL017015, 2003.

Michalski, G., Bhattacharya, S. K., and Mase, D. F.: Oxygen isotope dynamics of atmospheric nitrate and its precursor molecules, in: Handbook of environmental isotope geochemistry, Springer, New York, 613–635, 2012.

Michalski, G., Bhattacharya, S. K., and Girsch, G.: NOx cycle and the tropospheric ozone isotope anomaly: an experimental investigation, Atmospheric Chemistry and Physics, 14, 4935–4953, https://doi.org/10.5194/acp-14-4935-2014, 2014.

Morin, S., Sander, R., and Savarino, J.: Simulation of the diurnal variations of the oxygen isotope anomaly (Δ 17 O) of reactive atmospheric species, Atmospheric Chemistry and Physics, 11, 3653–3671, https://doi.org/10.5194/acp-11-3653-2011, 2011.

Nah, T., Sanchez, J., Boyd, C. M., and Ng, N. L.: Photochemical Aging of α-pinene and β-pinene Secondary Organic Aerosol formed from Nitrate Radical Oxidation, Environ. Sci. Technol., 50, 222–231, https://doi.org/10.1021/acs.est.5b04594, 2016.

https://doi.org/10.5194/egusphere-2024-3860
Preprint. Discussion started: 17 December 2024

Ng, N. L., Brown, S. S., Archibald, A. T., Atlas, E., Cohen, R. C., Crowley, J. N., Day, D. A., Donahue, N. M., Fry, J. L., Fuchs, H., Griffin, R. J., Guzman, M. I., Herrmann, H., Hodzic, A., Iinuma, Y., Jimenez, J. L., Kiendler-Scharr, A., Lee, B. H., Luecken, D. J., Mao, J., McLaren, R., Mutzel, A., Osthoff, H. D., Ouyang, B., Picquet-Varrault, B., Platt, U., Pye, H. O. T., Rudich, Y., Schwantes, R. H., Shiraiwa, M., Stutz, J., Thornton, J. A., Tilgner, A., Williams, B. J., and Zaveri, R. A.: Nitrate radicals and biogenic volatile organic compounds: oxidation, mechanisms, and organic aerosol, Atmos. Chem. Phys., 17, 2103–2162, https://doi.org/10.5194/acp-17-2103-2017, 2017.

Nozière, B., Barnes, I., and Becker, K.: Product study and mechanisms of the reactions of α-pinene and of pinonaldehyde with OH radicals, J. Geophys. Res., 104, 23645–23656, https://doi.org/10.1029/1999JD900778, 1999.

Orsini, D. A., Ma, Y., Sullivan, A., Sierau, B., Baumann, K., and Weber, R. J.: Refinements to the particle-into-liquid sampler (PILS) for ground and airborne measurements of water soluble aerosol composition, Atmospheric Environment, 37, 1243–1259, https://doi.org/10.1016/S1352-2310(02)01015-4, 2003.

Rindelaub, J. D., McAvey, K. M., and Shepson, P. B.: The photochemical production of organic nitrates from α-pinene and loss via acid-dependent particle phase hydrolysis, Atmospheric Environment, 100, 193–201, https://doi.org/10.1016/j.atmosenv.2014.11.010, 2015.

Rindelaub, J. D., Borca, C. H., Hostetler, M. A., Slade, J. H., Lipton, M. A., Slipchenko, L. V., and Shepson, P. B.: The acid-catalyzed hydrolysis of an α-pinene-derived organic nitrate: kinetics, products, reaction mechanisms, and atmospheric impact, Atmospheric Chemistry and Physics, 16, 15425–15432, https://doi.org/10.5194/acp-16-15425-2016, 2016.

Romer, P. S., Duffey, K. C., Wooldridge, P. J., Allen, H. M., Ayres, B. R., Brown, S. S., Brune, W. H., Crounse, J. D., De Gouw, J., and Draper, D. C.: The lifetime of nitrogen oxides in an isoprene-dominated forest, Atmospheric Chemistry and Physics, 16, 7623–7637, https://doi.org/10.5194/acp-16-7623-2016, 2016.

Russell, L. M., Bahadur, R., and Ziemann, P. J.: Identifying organic aerosol sources by comparing functional group composition in chamber and atmospheric particles, Proc. Natl. Acad. Sci. U.S.A., 108, 3516–3521, https://doi.org/10.1073/pnas.1006461108, 2011.

Sato, K., Ikemori, F., Ramasamy, S., Iijima, A., Kumagai, K., Fushimi, A., Fujitani, Y., Chatani, S., Tanabe, K., and Takami, A.: Formation of secondary organic aerosol tracers from anthropogenic and biogenic volatile organic compounds under varied NOx and oxidant conditions, Atmospheric Environment: X, 14, 100169, https://doi.org/10.1016/j.aeaoa.2022.100169, 2022.

Saunders, S. M., Jenkin, M. E., Derwent, R. G., and Pilling, M. J.: Protocol for the development of the Master Chemical Mechanism, MCM v3 (Part A): tropospheric degradation of non-aromatic volatile organic compounds, Atmospheric Chemistry and Physics, 3, 161–180, https://doi.org/10.5194/acp-3-161-2003, 2003.

Savarino, J., Morin, S., Erbland, J., Grannec, F., Patey, M. D., Vicars, W., Alexander, B., and Achterberg, E. P.: Isotopic composition of atmospheric nitrate in a tropical marine boundary layer, PNAS, 110, 17668–17673, https://doi.org/10.1073/pnas.1216639110, 2013.

https://doi.org/10.5194/egusphere-2024-3860
Preprint. Discussion started: 17 December 2024

Sigman, D. M., Casciotti, K. L., Andreani, M., Barford, C., Galanter, M., and Böhlke, J. K.: A bacterial method for the nitrogen isotopic analysis of nitrate in seawater and freshwater, Analytical chemistry, 73, 4145–4153, https://doi.org/10.1021/ac010088e, 2001.

Takeuchi, M. and Ng, N. L.: Chemical composition and hydrolysis of organic nitrate aerosol formed from hydroxyl and nitrate radical oxidation of α-pinene and β-pinene, Atmospheric Chemistry and Physics, 19, 12749–12766, https://doi.org/10.5194/acp-19-12749-2019, 2019.

Takeuchi, M., Berkemeier, T., Eris, G., and Ng, N. L.: Non-linear effects of secondary organic aerosol formation and properties in multi-precursor systems, Nat Commun, 13, 7883, https://doi.org/10.1038/s41467-022-35546-1, 2022.

Tuet, W. Y., Chen, Y., Xu, L., Fok, S., Gao, D., Weber, R. J., and Ng, N. L.: Chemical oxidative potential of secondary organic aerosol (SOA) generated from the photooxidation of biogenic and anthropogenic volatile organic compounds, Atmospheric Chemistry and Physics, 17, 839–853, https://doi.org/10.5194/acp-17-839-2017, 2017.

Vicars, W. C. and Savarino, J.: Quantitative constraints on the 17 O-excess (Δ 17 O) signature of surface ozone: Ambient measurements from 50° N to 50° S using the nitrite-coated filter technique, Geochimica et Cosmochimica Acta, 135, 270–287, http://dx.doi.org/10.1016/j.gca.2014.03.023, 2014.

Walters, W. W. and Hastings, M. G.: Triple oxygen stable isotope analysis of nitrite measured using continuous flow isotope ratio mass spectrometry, MethodsX, 11, 102413, https://doi.org/10.1016/j.mex.2023.102413, 2023.

Walters, W. W. and Michalski, G.: Theoretical calculation of nitrogen isotope equilibrium exchange fractionation factors for various NOy molecules, Geochimica et Cosmochimica Acta, 164, 284–297, https://doi.org/10.1016/j.gca.2015.05.029, 2015.

Walters, W. W. and Michalski, G.: Ab initio study of nitrogen and position-specific oxygen kinetic isotope effects in the NO + O3 reaction, The Journal of Chemical Physics, 145, 224311, https://doi.org/10.1063/1.4968562, 2016.

Walters, W. W., Simonini, D. S., and Michalski, G.: Nitrogen isotope exchange between NO and NO2 and its implications for δ15N variations in tropospheric NOx and atmospheric nitrate, Geophys. Res. Lett., 43, 2015GL066438, https://doi.org/10.1002/2015GL066438, 2016.

Walters, W. W., Fang, H., and Michalski, G.: Summertime diurnal variations in the isotopic composition of atmospheric nitrogen dioxide at a small midwestern United States city, Atmospheric Environment, 179, 1–11, https://doi.org/10.1016/j.atmosenv.2018.01.047, 2018.

Walters, W. W., Takeuchi, M., Ng, N. L., and Hastings, M. G.: Incorporating Oxygen Isotopes of Oxidized Reactive Nitrogen in the Regional Atmospheric Chemistry Mechanism, version 2 (ICOIN-RACM2), Geoscientific Model Development, 17, 4673–4687, https://doi.org/10.5194/gmd-17-4673-2024, 2024a.

https://doi.org/10.5194/egusphere-2024-3860
Preprint. Discussion started: 17 December 2024

Walters, W. W., Pye, H. O. T., Kim, H., and Hastings, M. G.: Modeling the Oxygen Isotope Anomaly (Δ17O) of Reactive Nitrogen in the Community Multiscale Air Quality Model: Insights into Nitrogen Oxide Chemistry in the Northeastern United States, ACS EST Air, https://doi.org/10.1021/acsestair.3c00056, 2024b.

Wang, Y., Piletic, I., Takeuchi, M., Xu, T., France, S., and Ng, N. L.: Synthesis and hydrolysis of atmospherically relevant monoterpene-derived organic nitrates, Environ Sci Technol, 55, 14595–14606, https://doi.org/10.1021/acs.est.1c05310, 2021.

Wang, Y., Takeuchi, M., Wang, S., Nizkorodov, S. A., France, S., Eris, G., and Ng, N. L.: Photolysis of Gas-Phase Atmospherically Relevant Monoterpene-Derived Organic Nitrates, J. Phys. Chem. A, 127, 987–999, https://doi.org/10.1021/acs.jpca.2c04307, 2023.

Wolfe, G. M., Marvin, M. R., Roberts, S. J., Travis, K. R., and Liao, J.: The Framework for 0-D Atmospheric Modeling (F0AM) v3.1, Geoscientific Model Development, 9, 3309–3319, https://doi.org/10.5194/gmd-9-3309-2016, 2016.

Xu, L., Suresh, S., Guo, H., Weber, R. J., and Ng, N. L.: Aerosol characterization over the southeastern United States using high-resolution aerosol mass spectrometry: spatial and seasonal variation of aerosol composition and sources with a focus on organic nitrates, Atmospheric Chemistry and Physics, 15, 7307–7336, 2015a.

Xu, L., Guo, H., Boyd, C. M., Klein, M., Bougiatioti, A., Cerully, K. M., Hite, J. R., Isaacman-VanWertz, G., Kreisberg, N. M., Knote, C., and others: Effects of anthropogenic emissions on aerosol formation from isoprene and monoterpenes in the southeastern United States (vol 112, pg 37, 2015), PROCEEDINGS OF THE NATIONAL ACADEMY OF SCIENCES OF THE UNITED STATES OF AMERICA, 112, E4509–E4509, 2015b.

Xu, L., Tsona, N. T., You, B., Zhang, Y., Wang, S., Yang, Z., Xue, L., and Du, L.: NOx enhances secondary organic aerosol formation from nighttime γ-terpinene ozonolysis, Atmospheric environment, 225, 117375, https://doi.org/10.1016/j.atmosenv.2020.117375, 2020.

Young, E. D., Galy, A., and Nagahara, H.: Kinetic and equilibrium mass-dependent isotope fractionation laws in nature and their geochemical and cosmochemical significance, Geochimica et Cosmochimica Acta, 66, 1095–1104, https://doi.org/10.1016/S0016-7037(01)00832-8, 2002.

Zare, A., Romer, P. S., Nguyen, T., Keutsch, F. N., Skog, K., and Cohen, R. C.: A comprehensive organic nitrate chemistry: insights into the lifetime of atmospheric organic nitrates, Atmospheric Chemistry and Physics, 18, 15419–15436, https://doi.org/10.5194/acp-18-15419-2018, 2018.